KfK 2907
Februar 1980

Use of Optical Model to Evaluate Fast Neutron Cross-Sections for Transactinide Nuclei

U. Fischer
Institut für Neutronenphysik und Reaktortechnik
Projekt Schneller Brüter

Kernforschungszentrum Karlsruhe

KERNFORSCHUNGSZENTRUM KARLSRUHE

Institut für Neutronenphysik und Reaktortechnik

Projekt Schneller Brüter

KfK 2907

Use of Optical Model to Evaluate Fast Neutron Cross-Sections for Transactinide Nuclei

U. Fischer

Kernforschungszentrum Karlsruhe GmbH, Karlsruhe

Kernforschungszentrum Karlsruhe GmbH
ISSN 0303-4003

Abstract

To evaluate Optical Model cross-sections, the Optical Model formalism is described. Adjusting the optical model parameters a sensitivity analysis is performed. Optical Model cross-sections assuming a spherical potential are evaluated for the nuclei U-238, Pu-240, Pu-242, Am-241 and Cm-244 taking into account the smooth A-dependence of these cross-sections. Computing the compound elastic cross-section σ_{CE} with the Hauser/Feshbach formula, and in one case with a semi-empirical method, the following types of cross-section are obtained: the total cross-section σ_{tot}, the elastic cross-section σ_{el}, the reaction cross-section σ_r and the differential elastic cross-section $\frac{d\sigma_{el}}{d\Omega}$. The evaluated cross-sections are compared to experimental data. Discrepancies in experimental and evaluated data are pointed out and recommendations are given. Furthermore capture cross-sections are evaluated based on the simple giant dipole resonance model.

Berechnung von Neutronenwirkungsquerschnitten einiger Transactinidenkerne im schnellen Bereich mit Hilfe des optischen Modells

Zusammenfassung

Zur Berechnung von Wirkungsquerschnitten mit dem optischen Modell wird der Formalismus des optischen Modells beschrieben. Zur Anpassung der Parameter des optischen Modells wird eine Sensitivitätsanalyse durchgeführt. Wirkungsquerschnitte nach dem optischen Modell werden für die Kerne U-238, Pu-240, Pu-242 Am-241 und Cm-244 berechnet, wobei ein sphärisches Potential zugrunde gelegt wird und die langsame A-Abhängigkeit dieser Querschnitte berücksichtigt wird. Nach Berechnung des compound-elastischen Querschnittes σ_{CE} nach der Hauser/Feshbach-Formel und in einem Fall nach einer semi-empirischen Methode werden folgende Querschnittstypen berechnet: der totale Wirkungsquerschnitt σ_{tot}, der elastische Wirkungsquerschnitt σ_{el}, der Reaktionsquerschnitt σ_r und der differentielle elastische Querschnitt $\frac{d\sigma_{el}}{d\Omega}$. Die berechneten Wirkungsquerschnitte werden mit experimentellen Werten verglichen. Diskrepanzen in den experimentellen wie in den evaluierten Daten werden deutlich gemacht und Empfehlungen werden gegeben. Überdies werden aufgrund des einfachen 'Giant-Dipole-Resonance-Modells' Capture-Querschnitte berechnet.

Contents

1. Introduction

Transactinide nuclei are in general highly radioactive and to some extent very shortlived. Therefore the measuring of neutron cross-sections of these nuclei is extremely complicated. In this situation evaluated cross-sections are useful to fill gaps of the measurements and sometimes they can even be used to verify existing experimental data.

From the upper keV - to the MeV - region the Optical Model is the most useful tool to evaluate average neutron cross-sections. The Optical Model parameters are adjusted to a suitable nucleus and, on the basis of the A-dependence, are extrapolated to other nuclei, for which experimental data are scarce or less accurate.

In this work the parameters are adjusted to the total cross-section of U-238, because U-238 is an even-even nucleus, for which a large amount of experimental data is available. On the other hand, for heavier even-even nuclei, which are the main object of consideration in this work, the measured cross-sections are scarce and partly less accurate.

Optical model cross-sections, for example the total cross-section σ_{tot} and the absorption cross-section σ_{abs}, depend smoothly on the mass number A. In the case of σ_{tot} in the mass region $232 \leq A \leq 239$ this can be seen from Fig. 1a and 1b, which are taken from Madland and Young /1/. Therefore it is possible to extrapolate cross-sections according to the A-dependence.

Theoretically this behaviour is confirmed by the terms for the average cross-sections derived from the optical model formalism. In the limiting case of low energies one obtains for the total cross-sections /2, 3/:

$$\bar{\sigma}_{tot} = 4\pi R'^2 + \frac{8\pi \cdot m}{k \cdot \hbar^2} \int W \cdot |u|^2 \, dr$$

Here R' is the scattering length for potential scattering, k the wave number, m the reduced mass from neutron and target nucleus, W the imaginary part of the potential and u the radial part of the wave function ψ for $l = 0$.

The ratio R'/R, where R is the potential radius, varies between A = 238 and A = 244 according to Feshbach /2/ between 1.08 and 1.06, resulting in a decrease of 4 % in R'^2. On the other hand, R^2 increases less than 2.5 % according to the $A^{2/3}$-behaviour. The variation of the second term in (1.1), which also depends according to the $A^{2/3}$-behaviour of the optical potential on A, is of the same order.

These reflections show that according to eq. (1.1) $\bar{\sigma}_{tot}$ should vary less than 4 % in the region 238 < A < 244. This behaviour is verified by this work (see sect. 3).

In contrast there are experimental data, which show large discrepancies. For instance, the total cross-section varies between A = 238 and A = 242 up to 35 %, being nearly ten times larger than the physically reasonable value. In the past evaluated cross-sections in the transactinide region often ignored the A-systematics shown above. Therefore they are partly very discrepant.

The present evaluation was performed with a spherical optical potential, in spite of the fact, that the nuclei considered are strongly deformed. It was shown, however, that the neutron cross-sections in the energy region from 10 keV to 15 MeV can be evaluated with this simple model quite satisfactorily. Furthermore, the work of Madland and Young, cited above, shows, that a coupled-channel-calculation with deformed potential scarcely produces better results.

2. The Optical Model

Nuclear reactions are many-body-problems, the incident particle interacting with the nucleons of the target nucleus. The optical model approximates the many-body-problem by a two-body-problem. The target nucleus acts with the average potential V(r) upon the incident particle. The particle's motion in the potential V(r) is given by the Schrödinger equation:

$$\Delta\psi + \frac{2m}{\hbar^2}(E - V(r))\psi = 0 \qquad (2.1)$$

Here E is the incident particle's energy in the center-of-mass system.

The first efforts to replace the target nucleus by a potential well were undertaken by Bethe in 1933 /4/. However, Bethe's potential well model failed to explain the narrow resonances in the low energy region. On the other hand, the compound nucleus theory developed by Niels Bohr soon afterwards /5/ was able to explain these narrow resonances on the basis of nucleon-nucleon interactions. According to the compound nucleus theory, the incident particle is absorbed by the target nucleus distributing its energy after a short time (ca. 10^{-16}s) equally among all nucleons. So the incident particle loses its identity during the compound state, the compound nucleus decaying independent of its formation. In this process the incident particle has a short mean free path compared to the radius of the nucleus. This results from the strong interaction with the nucleons of the target nucleus.

After World War II cross-section measurements in the MeV region became possible and the experimentalists (e.g. /6/) discovered resonances having widths in the order to some MeV, whereas the widths of the compound-resonances lie in the order eV to keV. These so-called giant resonances depend on the mass number A and on the incident energy E. Because only a potential well model is able to explain the giant resonances, the optical model was stressed again /7, 8/. In order to take into account the absorption and therefore the formation of the compound nucleus, the potential was made complex. So the absorption is given by the imaginary part of the potential W(r). This was done in analogy to optics, where a complex index

of refraction is used to describe the refraction and absorption of light propagating through a refractive medium.

In this case, the incident particle possesses a mean free path comparative with the radius of the nucleus. Therefore, resonances can occur in the potential well at particular values of the wave length.

These single-particle-resonances depend on the potential radius R and on the wave number inside the potential well K. For example, a square well potential of the form

$$V(r) = \begin{cases} -V_o & r \leq R \\ 0 & r > R \end{cases}$$

where the potential depth according to the Fermi-gas-model is of the order of 45 MeV and the potential radius according to the $A^{1/3}$-law is $R = 1.2 \cdot A^{1/3}$, yield resonances for /9/:

$$K \cdot R = (n + \frac{1}{2})\pi$$

with n even, l = angular momentum quantum number

Up to high energies, the compound nucleus theory had to be completed by the optical model. The optical potential, however, is an average potential of all nucleons of the target nucleus. Therefore the optical model is unable to reproduce the precise structure of the cross-sections. Rather the optical model yields average cross-sections. Up to high energies, however, the compound resonances become unresolvable and in this region the optical model cross-sections agree with the measured cross-sections.

To yield the cross-sections evaluable with the optical model, the compound resonances therefore have to be averaged. In the following the derivation of the average cross-section and the association with measurable cross-sections is given.

2.1 Average Cross-Sections

The scattering of a spinless particle at a spinless nucleus is considered in the following. The wave functions $\psi(\vec{r})$ of the particle considered asymptotically consists of the incident plane wave (in z-direction) e^{ikz} and the scattered spherical wave:

$$\psi(\vec{r}) = A(e^{ikz} + \frac{f(\theta)}{r} \cdot e^{ikr}) \tag{2.2}$$

Herein A is a constant to be normed, θ is the scattering angle and r is the distance particle-nucleus. So the scattering is described by the scattering amplitude $f(\theta)$. The total cross-section σ_{tot} is obtained according to the optical theorem (e.g. Schiff /10/) from the imaginary part of the scattering amplitude in forward direction:

$$\sigma_{tot} = \frac{4\pi}{k} \mathrm{Im}[f(0)] \tag{2.3}$$

The differential cross-section for elastic scattering is given by the absolute square of the scattering amplitude /10/:

$$\frac{d\sigma_{el}}{d\Omega} = |f(\theta)|^2 \tag{2.4}$$

Therefore the elastic cross-section is given by:

$$\sigma_{el} = \int \left(\frac{d\sigma_{el}}{d\Omega} \right) d\Omega = \int |f(\theta)|^2 d\Omega \tag{2.5}$$

The reaction cross-section σ_r is finally obtained in the following manner:

$$\sigma_r = \sigma_{tot} - \sigma_{el} \tag{2.6}$$

Provided that the energy resolution is good, the scattering amplitude $f(\theta)$ fluctuates strongly, dependent on the incident particle's energy E. This is so, because $f(\theta)$ describes the exact structure of the cross-sections. The optical model scattering amplitude, however must be an average amplitude, for optical model cross-sections are average cross-sections. Therefore

$f(\theta)$ must be averaged over an interval Δ which is large compared to the widths of the compound resonances, but small compared to the widths of the giant resonances:

$$\overline{f(E)} = \frac{1}{\Delta} \int_{E-\frac{\Delta}{2}}^{E+\frac{\Delta}{2}} f(E')dE' \qquad (2.7)$$

Now the optical potential is that potential, for which $\overline{f(\theta)}$ is the scattering amplitude. According to eq. (2.3) σ_{tot} depends linearly on $f(\theta)$. This yields for $\tilde{\sigma}_{tot}$ (following Hodgson /11,12/ the optical model cross-sections are signed with a tilde):

$$\tilde{\sigma}_{tot} = \frac{4\pi}{k} \mathrm{Im}\left[\overline{f(\theta)}\right] \qquad (2.8)$$

i.e. $$\tilde{\sigma}_{tot} = \overline{\sigma_{tot}} \qquad (2.9)$$

The optical model total cross-section agrees with the average total cross-section.

For the elastic cross-section according to eq. (2.5) is valid:

$$\tilde{\sigma}_{el} = \int |\overline{f(\theta)}|^2 d\Omega \qquad (2.10)$$

But $\tilde{\sigma}_{el}$ disagrees with $\bar{\sigma}_{el}$, which is defined as follows:

$$\bar{\sigma}_{el} = \int \overline{|f(\theta)|^2} d\Omega \qquad (2.11)$$

The difference, the so-called fluctuation cross-section σ_{fl}, is given by the angle-integrated average fluctuation square:

$$\sigma_{fl} = \bar{\sigma}_{el} - \tilde{\sigma}_{el} = \int \left\{ \overline{|f(\theta)|^2} - |\overline{f(\theta)}|^2 \right\} d\Omega \qquad (2.12)$$

With eq. (2.6) $\tilde{\sigma}_r$ is given by:

$$\tilde{\sigma}_r = \tilde{\sigma}_{tot} - \tilde{\sigma}_{el} = \bar{\sigma}_{tot} - \bar{\sigma}_{el} + \sigma_{fl} = \bar{\sigma}_r + \sigma_{fl} \qquad (2.13)$$

therefore:

$$\tilde{\sigma}_r = \bar{\sigma}_r + \sigma_{fl} \tag{2.14a}$$

$$\tilde{\sigma}_{el} = \bar{\sigma}_{el} - \sigma_{fl} \tag{2.14b}$$

The average reaction cross-section $\bar{\sigma}_r$ includes all reactions, therefore σ_{fl} represents an elastic cross-section. On the other hand, $\tilde{\sigma}_r$ contains σ_{fl}, and especially for $\bar{\sigma}_r = 0$, i.e. there are no reactions, $\tilde{\sigma}_r$ is totally given by σ_{fl}, concluding that σ_{fl} is an absorptive cross-section. So σ_{fl} represents that part of the elastic scattering, where the incident particle is first absorbed, leading to the formation of the compound nucleus, but then is emitted back into the entrance channel. Therefore σ_{fl} is given by the average compound elastic cross-section $\bar{\sigma}_{CE}$, that can be shown also by explicit averaging over Breit-Wigner resonances (e.g. Hodgson /11, 12/).

On the other hand, $\tilde{\sigma}_{el}$ represents the pure potential scattering, the incident particle being only scattered by the target nucleus, but not absorbed. Therefore $\tilde{\sigma}_{el}$ is called in general the shape elastic cross-section σ_{SE}.

$\tilde{\sigma}_r$ is the total absorption cross-section (including the average compound elastic cross-section) being identical with the compound nucleus formation cross-section σ_c. This also can be shown strictly mathematically.

For the optical model cross-sections now the following equations are valid:

$$\tilde{\sigma}_{tot} = \bar{\sigma}_{tot} \tag{2.15a}$$

$$\tilde{\sigma}_r = \sigma_{abs} = \bar{\sigma}_r + \bar{\sigma}_{CE} = \bar{\sigma}_c \tag{2.15b}$$

$$\tilde{\sigma}_{el} = \sigma_{SE} = \bar{\sigma}_{el} - \bar{\sigma}_{CE} \tag{2.15c}$$

Only the average cross sections $\bar{\sigma}_{tot}$, $\bar{\sigma}_r$ and $\bar{\sigma}_{el}$ can be measured. Therefore the average total cross-section is the only cross-section evaluable with the optical model and simultaneously measurable by experiment. So σ_{tot} is highly

suitable for parameter adjustment (comp. sect. 3.1).

The experimentally measurable reaction cross-section $\bar{\sigma}_r$ however cannot be evaluated directly by the optical model. The optical model yields the absorption cross-section $\tilde{\sigma}_r = \sigma_{abs}$. In order to calculate $\bar{\sigma}_r$ and compare with experimental results, $\bar{\sigma}_{CE}$ must be known (cf. sect. 2.2).

By averaging the elastic cross-section is split into the compound elastic part $\bar{\sigma}_{CE}$ and into the shape elastic part σ_{SE}. Experimentally however σ_{SE} and $\bar{\sigma}_{CE}$ cannot be separated. Measured is the quantity:

$$\bar{\sigma}_{el} = \sigma_{SE} + \bar{\sigma}_{CE} = \tilde{\sigma}_{el} + \bar{\sigma}_{CE}$$

As in the case of $\bar{\sigma}_r$, comparison with experimental results can only be done if $\bar{\sigma}_{CE}$ is known.

In the high energy region (E > ca. 7 MeV) $\bar{\sigma}_{CE}$ however decreases rapidly towards zero. This is so, because up to high energies more and more outgoing channels are opening, especially a lot of competing inelastic channels open, and therefore the probability of the particle considered being scattered into the compound elastic channel becomes extremely small. Moreover, at high energies the direct processes become significant, outweighing the compound elastic part of the scattering. So above 7 MeV holds:

$$\sigma_{abs} = \bar{\sigma}_r \quad \text{and} \quad \sigma_{SE} = \bar{\sigma}_{el} \qquad E \geq 7 \text{ MeV}$$

2.2 Determination of σ_{CE}

To obtain σ_{CE} there are on principle two distinct methods applicable:

a) The Hauser/Feshbach formula

The Hauser/Feshbach formula /13/ yields the cross-section $\sigma_{\alpha\beta}$ for a reaction going via the compound nucleus from channel α to channel β:

$$\sigma_{\alpha\beta} = \frac{\pi}{k_\alpha^2} \sum_{J,l} g^J \frac{T_\alpha T_\beta}{\sum_{\beta'} T_{\beta'}} \qquad (2.16)$$

Here are:

$$g^J = \frac{2J+1}{(2i+1)(2I+1)}$$ the spin weighting factor

i = the incident particle's spin quantum number

I = the target nucleus' spin quantum number

J is the total angular momentum quantum number, which sums up according to the sum rule for the angular momentum: $\vec{J} = \vec{I} + \vec{i} + \vec{l}$

l = angular momentum quantum number of the incident particle

$T_\alpha = 1 - |\eta_\alpha|^2$: Transmission coefficient being calculated by the optical model (η_α is explained in sect. 2.5).

The first sum in (2.16) takes into account all allowed angular momentum combinations, the sum $\sum_{\beta'} T_{\beta'}$ in the denominator of (2.16) extends over all energetically possible channels.

The Hauser/Feshbach formula (2.16) is clarified by writing

$$\sigma_{c,\alpha} = \frac{\pi}{k_\alpha^2} \sum_{J,l} g^J \cdot T_\alpha^J \qquad P_\beta = \frac{T_\beta}{\sum_{\beta'} T_{\beta'}}$$

when $\sigma_{c,\alpha}$ is the compound nucleus formation cross-section via channel α and P_β is the probability for decaying into channel β. Therefore the Hauser/Feshbach formula can be written in the following form illustrating the compound nucleus process:

$$\sigma_{\alpha,\beta} = \sigma_{c,\alpha} \cdot P_\beta$$

The compound elastic cross-section is gained from (2.16) by putting $\alpha = \beta$:

$$\bar{\sigma}_{CE} = \sigma_{\alpha\alpha} = \frac{\pi}{k_\alpha^2} \cdot \sum_{J,l} g^J \cdot \frac{T_\alpha^2}{\sum_{\beta'} T_{\beta'}} \qquad (2.17)$$

However, to get $\bar{\sigma}_{CE}$ via eq. (2.17) the compound nucleus' energy levels must be known, or if they are missing a level density formula must be applied (cf. sect. 2.6).

b) Semi-empirical method

If there are enough reliable cross-section data for the interesting nucleus it is possible to get σ_{CE} by a semi-empirical method. To do this, the optical model parameters are first adjusted to suitable cross-sections. Often the differential elastic cross-section at high energies, where $\bar{\sigma}_{CE}$ is zero, is used for adjusting /14/. With the parameters gained $\frac{d\sigma_{el}}{d\Omega}$ is then evaluated in the low energy region. Finally one gets $\frac{d\sigma_{CE}}{d\Omega}$, assumed to be isotropic, by subtracting the evaluated data from the experimental ones. This procedure is done for several energies to get the energy dependence of σ_{CE}.

Another way to get σ_{CE} by a semi-empirical method is followed in this work. Here the parameter adjusting is done at the total cross-section. This has the advantage, that the adjusting can be executed over the whole energy region of interest. $\bar{\sigma}_{CE}$ can be gained simply by doing the difference

$$\bar{\sigma}_{CE} = \sigma_{abs} - \sigma_{ne}^{exp} \tag{2.18}$$

where σ_{abs} is the absorption cross-section calculated with the adjusted parameters from the optical model and σ_{ne}^{exp} is the experimental non-elastic cross-section. To see the accuracy of the evaluated $\bar{\sigma}_{CE}$ values, the elastic cross-section $\bar{\sigma}_{el}$ can be computed according to

$$\bar{\sigma}_{el} = \sigma_{SE} + \bar{\sigma}_{CE}$$

and so can be compared to measured σ_{el}-data. Furthermore, if experimental $\frac{d\sigma}{d\Omega}$ data are available, $\frac{d\sigma_{el}}{d\Omega}$ can be obtained by adding to $\frac{d\sigma_{SE}}{d\Omega}$ the isotropic differential compound elastic cross-section and so can be compared with measured data:

$$\frac{d\sigma_{CE}}{d\Omega} = \frac{\bar{\sigma}_{CE}}{4\pi} \tag{2.19}$$

$$\frac{d\sigma_{el}}{d\Omega} = \frac{d\sigma_{SE}}{d\Omega} + \frac{\bar{\sigma}_{CE}}{4\pi} \tag{2.20}$$

In the present work $\bar{\sigma}_{CE}$ is evaluated both with the Hauser/Feshbach formula and with the semi-empirical method after adjusting the parameters to σ_{tot}. The results are compared in Fig. 3. In section 3.1 this point will be considered in greater detail.

2.3 Form of the Optical Model

The optical potential used in this work is based on the work of Wilmore and Hodgson /15/ (cf. also sect. 2.4). The potential consists of a real part V(r) and an imaginary part W(r). A coulomb term is not included, since only neutron-induced reactions are considered. Further a spin orbit term is not taken into account since this is hardly significant /11, 12/, except in the case of polarization being not considered here. The form of the optical model therefore is as follows:

$$U(r) = - V \cdot f(r) - i \cdot W \cdot g(r) \tag{2.21}$$

Herein V is the real and W the imaginary potential depth, f(r) and g(r) are the form factors giving the form and radial dependence of the potential. Especially f(r) is of the Woods-Saxon form:

$$f(r) = \frac{1}{1 + e^{\frac{r-R_r}{a_r}}} \tag{2.22}$$

where R_r is the real potential radius: $R_r = r_r \cdot A^{1/3}$ and a_r is the real diffuseness.

The imaginary form factor g(r) is of a derivated Woods-Saxon form having its maximum at $r = R_i$. This choice is based on the fact, that the absorption takes place mainly at the surface of the nucleus /11/.

$$g(r) = -4 \cdot a_i \cdot \frac{d}{dr} f(r) = \frac{4 \cdot e^{\frac{r-R_i}{a_i}}}{\left(1 + e^{\frac{r-R_i}{a_i}}\right)^2} \tag{2.23}$$

where R_i is the radius of the imaginary potential well: $R_i = r_i \cdot A^{1/3}$ and a_i is the imaginary diffuseness.

So the optical model parameters free for adjusting are in this case:

$$V,\ W,\ r_r,\ r_i,\ a_r,\ a_i$$

If the evaluation is performed over a large energy region, using a local potential, it is necessary to choose the potential depths V and W energy dependent (cf. sect. 2.4), e.g.:

$$V = V_o + V_i \cdot E + V_2 \cdot E^2$$

$$W = W_o + W_i \cdot E$$

So the parameters V_1, V_2 and W_1 are to be adjusted additionally.

The optical model parameters, free for adjusting, clearly are "free" only within physically reasonable limits. So the real potential depth V must be of the order 40 - 50 MeV (according to the Fermi gas model giving a Fermi energy of ca. 30 MeV, assuming a neutron separation energy of ca. 10 MeV, V is of the order of 40 MeV). The real radius parameter r_r must have a value near 1.2 fm, which is deduced from experiments.

Furthermore, there are so-called optical model ambiguities arising from the fact, that different values of certain parameters produce the same results. For instance, a real potential depth of ca. 47 MeV can yield σ_{tot}-values in good agreement with experimental values, but V ≈ 80 MeV or V ≈ 120 MeV can also produce such agreement. Clearly, the last two potential depths are physically unreasonable. Another example is the $V \cdot r^n$ ambiguity, where n is ca. 2. This means that the results from optical model calculations are not changed when changing V or r in such a manner that $V \cdot r^n = \text{const}$. So if the agreement is optimal for $V = V_1$ and $r = r_1$, the same agreement will be obtained choosing $V = V_2$ and $r = r_2$ with $V_2 \cdot r_2^n = V_1 \cdot r_1^n$.

Now adjusting optical model parameters, it is clear that several ambiguities are to be studied in order to gain the physically reasonable parameters.

However in the case of this work the physically well-established Wilmore/ Hodgson parameters (cf. sect. 2.4) are used as starting point in the adjusting procedure and finally they are only slightly changed (cf. sect. 3.1.1). Therefore a detailed ambiguity study is not performed here. A discussion of the optical model ambiguities is given e.g. by Hodgson /11, 12/, a detailed analysis in the case of ^{3}He-scattering at light nuclei is given by Schelinsky et al. /29/.

2.4 Perey/Buck potential and Wilmore/Hodgson approximation

The optical potential can be derived from the microscopic many-body-problem, as was done by Feshbach /2/. There the potential sums up all the individual interactions of the incident particle with each nucleon of the target nucleus. Now in deriving an average potential, i.e. an optical potential, Feshbach showed this potential to be non-local in character. So the potential acting upon the incident particle not only depends on the distance r target nucleus-particle but is also influenced by the wave function $\psi(r')$ of the particle and therefore depends on both r and r'. The potential thus becomes momentum-dependent.

In the Schrödinger equation the term:

$$V(\vec{r}) \cdot \psi(\vec{r})$$

describing the interaction particle - target nucleus changes into:

$$\int V(\vec{r},\vec{r}') \, \psi(\vec{r}') \, d\vec{r}'$$

Hence the Schrödinger equation

$$\left\{ \frac{\hbar^2}{2m} \Delta + E \right\} \psi(\vec{r}) = V(\vec{r}) \, \psi(\vec{r}) \qquad (2.24)$$

changes into the following integro-differential equation:

$$\left\{ \frac{\hbar^2}{2m} \Delta + E \right\} \psi(\vec{r}) = \int V(\vec{r},\vec{r}') \, \psi(\vec{r}') \, d\vec{r}' \qquad (2.25)$$

Here $V(\vec{r},\vec{r}')$ is the non-local potential. Perey and Buck showed /14/, that in using this non-local potential no energy dependence of the potential is needed to reproduce neutron cross-sections. However the integro-differential equation (2.25) is difficult to handle. It can be solved only with enormous effort by numerical integration and iteration. But Perey and Buck also showed that if certain conditions are fulfilled, there is an equivalent local potential $V_L(r)$ corresponding to the non-local potential $V_N(r)$ satisfying the following equation:

$$V_L(r) \exp\left\{ \frac{m\beta^2}{2\hbar^2} (E - V_L(r)) \right\} = V_N(r) \qquad (2.26)$$

where β is the range of the non-locality.

Wilmore and Hodgson solved this equation by iteration /15/. They showed that already the first approximation for $V_L(r)$ is sufficient. The parameters gained by this procedure show the following energy- and A-dependence, being equivalent to the non-locality (2.25):

$$U = 47.01 \text{ MeV} - 0.267 \cdot E - 0.00118 \frac{E^2}{\text{MeV}} \qquad (2.27)$$

$$W = 9.52 \text{ MeV} - 0.53 \cdot E \qquad E \text{ in MeV}$$

$$r_r = 1.32 - 0.00076 \cdot A + 10^{-6} A^2 - 8 \cdot 10^{-5} A^3 \text{ (fm)}$$

$$r_i = 1.266 - 0.0037 \cdot A + 2 \cdot 10^{-6} A^2 - 4 \cdot 10^{-5} A^3 \text{ (fm)}$$

$$a_r = 0.66 \text{ fm} \qquad a_i = 0.48 \text{ fm}$$

With these parameters and the corresponding potential, using the Woods-Saxon form factors described in sect. 2.3, Wilmore and Hodgson succeeded in reproducing neutron cross-sections over a large A- and E-region. However in the actinide region, where U-238 was considered, the results were less successful. Nevertheless, the Wilmore/Hodgson parameters are used as a starting point in this work. As described in sect. 3.1.1, the parameters had to be changed slightly for the nuclei considered.

2.5 The basic formulae and the procedure for computing the optical model cross-sections

To obtain the cross-sections, the Schrödinger equation (2.24) must be solved with the potential (2.21). To do this, a partial wave analysis is performed yielding for the present assumed case of a spinless particle (no spin-orbit interaction) the following differential equation for the partial $u_l(r)$ $\left(u(r) = r \cdot \psi(r)\right)$:

$$\frac{d^2}{dr^2} u_l(r) + \left\{k^2 - \frac{2m}{\hbar^2} \cdot V(r) - \frac{l(l+1)}{r^2}\right\} u_l(r) = 0 \qquad (2.28)$$

with $k^2 = \frac{2m}{\hbar^2} \cdot E$

The cross sections then are /16/:

$$\sigma_{tot} = \frac{2\pi}{k^2} \sum_l (2l+1)(1-\mathrm{Re}[\eta_l]) \qquad (2.29a)$$

$$\sigma_{SE} = \frac{\pi}{k^2} \sum_l (2l+1)\,|1-\eta_l|^2 \qquad (2.29b)$$

$$\sigma_{abs} = \frac{\pi}{k^2} \sum_l (2l+1)(1-|\eta_l|^2) \qquad (2.29c)$$

Here the eigenvalue of the scattering natrix η_l describes the change in phase and amplitude of a partial wave scattered by the potential V(r). The scattering amplitude $f(\theta)$ is associated with η_l according to the following Legendre expansion:

$$f(\theta) = \frac{i}{2k} \sum_l (2l+1)(1-\eta_l) P_l(\cos\theta) \qquad (2.30)$$

where $P_l(\cos\theta)$ is the Legendre polynomial of order l.

The differential cross-section therefore reads:

$$\frac{d\sigma}{d\Omega} = |f(\theta)|^2 = \frac{1}{4k^2} \left|\sum_l (2l+1)(1-\eta_l) P_l(\cos\theta)\right|^2 \qquad (2.31)$$

The calculations were performed with the computer code HAUSER*4 /17/. However the program had to be modified, since in its original version only reaction cross-sections could be calculated (cf. sect. 3.1).

The modified version, called HAUSER*4/MOD, is able to calculate η_l and according to eq. (2.29 a - c) σ_{tot}, σ_{SE} and σ_{abs}. Furthermore, a subroutine was implemented, which enables computing the differential shape elastic cross-section for spinless particles according to eq. (2.31).

The radial Schrödinger equation (2.28) with the potential (2.21) is solved numerically with the Cowell method /18, 19, 20/. In this procedure the function $u_l(r)$ is obtained at the points r and Δr. Outside the range of the potential (V(r) is set equal zero for $r \geq r_m$, the matching radius r_m is chosen to be twice the value of the potential radius R) for $u_l(\rho_m) = u_l(k \cdot r_m)$ the following analytical term is obtained /12, 16, 20/:

$$u_l(\rho_m) \sim F_l(\rho_m) + i \cdot G_l(\rho_m) + \eta_l\left[F_l(\rho_m) - i\, G_l(\rho_m)\right] \qquad (2.32)$$

$F_l(\rho)$ and $G_l(\rho)$ are Bessel resp. Neumann functions as being defined e.g. in Schiff p. 85 /10/ or Messiah appendix B.2 /9/. Together with the values of $u_l(\rho_m)$ and $u_l(\rho_n) = u_l(\rho_m + \Delta\rho)$ gained by numerical integration of eq. (2.28), η_l is obtained from the ratio

$$\frac{u_l(\rho_m)}{u_l(\rho_n)} = \frac{F_l(\rho_m) + i\, G_l(\rho_m) + \eta_l\left[F_l(\rho_m) + i\, G_l(\rho_m)\right]}{F_l(\rho_n) + i\, G_l(\rho_n) + \eta_l\left[F_l(\rho_n) + i\, G_l(\rho_n)\right]}$$

yielding for η_l:

$$\eta_l = \frac{u_l(\rho_m)\cdot\left[F_l(\rho_n) + i\, G_l(\rho_n)\right] - u_l(\rho_n)\left[F_l(\rho_m) + i\, G_l(\rho_m)\right]}{u_l(\rho_n)\left[F_l(\rho_m) - i\, G_l(\rho_m)\right] + u_l(\rho_m)\left[F_l(\rho_n) - i\, G_l(\rho_n)\right]} \qquad (2.33)$$

Now knowing η_l the cross-sections (2.29 a - c) can be evaluated. Furthermore the particle transmission coefficients are obtained according to

$$T_l = 1 - |\eta_l|^2 \qquad (2.34)$$

and so can be used in the Hauser/Feshbach formula (2.16).

However to do the sum in the denominator of (2.16) besides the particle transmission coefficients, the capture, and in the high energy region, the fission transmission coefficients contribute an essential part. The procedure to obtain the capture transmission coefficients is described in sect. 2.6. The evaluation of the fission transmission cross-sections is described in the following only briefly because fission cross-sections are not considered in this work. The fission transmission coefficients used in (2.10) for calculating σ_{CE} and $\sigma_{n,\gamma}$ are obtained according to Hill and Wheeler /21/:

$$T_f = \frac{1}{1 + \exp\{\frac{E-E_1}{\hbar\omega_1}\}} \tag{2.35}$$

where the fission barrier is assumed to be an inverse oscillator potential of height E_1 and width $\hbar\omega_1$. Taking into account the double-humped barrier is done by calculating the transmission coefficient T_A resp. T_B individually for each barrier and taking an average transmission coefficient according to:

$$\bar{T}_f = \frac{T_A \cdot T_B}{T_A + T_B} \tag{2.36}$$

2.6 The capture cross-section

Besides optical model cross-sections capture cross-sections are considered in this work. The partial capture cross-sections $\sigma_{n,\gamma}(\varepsilon_\gamma)$, where ε_γ is the photon energy, are obtained from the Hauser/Feshbach formula (2.16) setting $T_\beta = T_\gamma$. The capture transmission coefficients are computed according to Holmes and Woosley /23/:

$$T_{E1}(\varepsilon_\gamma) = 2\pi \cdot \frac{4}{3\pi} \cdot \frac{N \cdot Z}{A} \cdot \frac{e^2}{\hbar c} \cdot \frac{K_E}{M_p c^2} \cdot \varepsilon_\gamma^{\,3} \cdot f_E(\varepsilon_\gamma)$$

$$= 5.185 \cdot 10^{-6} A \cdot K_E \cdot \varepsilon_\gamma^{\,3} \cdot f_E(\varepsilon_\gamma) \tag{2.37}$$

for E1-radiation and

$$T_{M1}(\varepsilon_\gamma) = 15\pi \cdot \frac{e^2}{\hbar c} \cdot \frac{1}{M_p^2 c^4} \cdot K_M \cdot \varepsilon_\gamma^3 \, f_M(\varepsilon_\gamma)$$

$$\approx 3.906 \cdot 10^{-7} \, K_M \cdot \varepsilon_\gamma^3 \cdot f_M(\varepsilon_\gamma) \qquad (2.38)$$

for M1-radiation. Only E1 and M1 radiation are assumed to contribute to the capture transmission coefficient, because higher polarities are very unlikely below 25 MeV /25/.

The constants in (2.37) resp. (2.38) are: N = number of neutrons, Z = number of protons, A = N+Z, M_p = proton mass, c = speed of light, e = elementary charge. K_E and K_M are parameters free for adjusting at experimental data. Holmes and Woosley used 0.25 for K_E and 0.05 for K_M. However, as is described in sect. 3.4 K_E had to be changed in this work.

$f_E(\varepsilon_\gamma)$ resp. $f_M(\varepsilon_\gamma)$ is the profile function reading in the case of E1 radiation according to the "giant dipole resonance model" /24, 25/ as follows:

$$f_E(\varepsilon_\gamma) = \frac{\Gamma_{GDR} \cdot \varepsilon_\gamma}{(\varepsilon_\gamma^2 - \varepsilon_{GDR}^2)^2 + (\Gamma_{GDR} \cdot \varepsilon_\gamma)^2} \qquad (2.39)$$

and in the case of M1 radiation is reduced to a constant according to the Weisskopf model:

$$f_M(\varepsilon_\gamma) = 1$$

For the width of the giant dipole resonance Γ_{GDR} and the resonance energy ε_{GDR} the values given by Holmes and Woosley /23/ are taken:

$$\varepsilon_{GDR} = \frac{35}{A^{1/6}} \quad \text{(MeV)}$$

$$\Gamma_{GDR} = \frac{33}{A^{1/3}} \quad \text{(MeV)} \qquad (2.40)$$

To calculate the total capture cross-section $\sigma_{n,\gamma}$ the transmission coefficients $T_{E1,M1}(\varepsilon_\gamma)$ must be summed up over all decay energies ε_γ, in the continuum $T_{E1,M1}(\varepsilon_\gamma)$ has to be weighted with the level density and integrated over the corresponding energy region:

$$T^{J^\pi} = \sum_i T_i^{J^\pi} + \int_{E_l}^{E^*} T_{E1,M1}^{J^\pi}(E^*-E')\rho(E')dE' \qquad (2.41)$$

Here E^* is the maximum excitation energy of the compound nucleus composed of the incident neutron energy E_n and the neutron binding energy:

$$E^* = E_n + B_n \qquad (2.42)$$

E' is the excitation energy:

$$E' = E^* - \varepsilon_\gamma \qquad (2.43)$$

and E_l the energy of the highest discrete level of the compound nucleus.

The level density $\rho(E')$, needed in eq. (2.41) as in the Hauser/Feshbach formula above the known discrete levels, is represented according to Gilbert and Cameron /26/. For high energies $E > E_x$ (E_x is defined below) the "back shifted Fermi gas formula" is used:

$$\sigma(E,J^\pi) = (2J+1)e^{-\frac{J(J+1)}{2\sigma^2}} \cdot \frac{e^{2\sqrt{a(E-\Delta)}}}{24\sqrt{2}\,a^{1/4}(E-\Delta)^{5/4}} \qquad (2.44)$$

For energies $E < E_x$ the "constant temperature formula" is adopted:

$$\rho(E) = \frac{1}{T} e^{\frac{E-E_o}{T}} \qquad (2.45)$$

The density parameters are computed following Gilbert and Cameron:

$$a = (0.00917 \cdot S + 0.120)\cdot A \quad (MeV^{-1}) \qquad (2.46a)$$

where $S = S(Z) + S(N)$ is a shell correction depending on the neutron number N and the proton number Z. S(Z) and S(N) are tabulated in the Gilbert/Cameron paper /26/.

The pairing energy is calculated from:

$$\Delta = P(Z) + P(N) \tag{2.46b}$$

P(Z) and P(N) also are taken from /26/.

The spin cut-off parameter σ is given by:

$$\sigma^2 = 0.0888 \sqrt{a(E-\Delta)} \cdot A^{2/3} \tag{2.46c}$$

The energy E_x at the matching point, where the formulae (2.44) and (2.45) are connected, is obtained by:

$$E_x = 2.5 + \frac{150}{A} + \Delta \quad \text{(MeV)} \tag{2.46d}$$

The nuclear temperature T in (2.45) is given by:

$$\frac{1}{T} = \sqrt{\frac{a}{E-\Delta}} - \frac{3}{2(E-\Delta)} \tag{2.46e}$$

Finally the referring energy E_o in (2.45) is obtained by:

$$E_o = E_x - T \cdot \ln\{T \cdot \rho_{Fermi}(E_x-\Delta)\} \tag{2.46f}$$

where ρ_{Fermi} is the Fermi level density given by (2.44).

The parameters calculated according to the formulae above are given in Tab. II. The capture cross-section calculations are described and discussed in sect. 3.4.

3. Cross-Section Evaluation and Interpretation

3.1 U-238 cross-sections

3.1.1 Parameter adjusting and sensitivity analysis for σ_{tot} of U-238

For the optical model parameter adjusting the nucleus U-238 is chosen for being that even-even nucleus with the highest mass number, for which still the most reliable experimental data of σ_{tot} are available. The values of σ_{tot} used for adjusting are those from the Kerndatenbibliothek Karlsruhe 3 KEDAK-3, where experimental data of several groups are taken into account /27/.

As a starting point, the Wilmore/Hodgson parameter (2.27) are used in HAUSER*4/MOD to obtain σ_{tot}. However the agreement to the KEDAK-3 data is very unsatisfactory. So a new parameter adjustment has to be performed.

The parameter adjusting is done in two steps. First the optical model code ABACUS /28/ is used to obtain a first set of improved parameters. The code ABACUS is able to do an automatic parameter search by varying simultaneously up to five parameters to minimize the quantity:

$$\chi^2 = \frac{1}{N} \sum_{i=1}^{N} \left\{ \frac{\sigma_i^{th} - \sigma_i^{exp}}{\sigma_i^{exp}} \right\}^2 \qquad (3.1)$$

where σ_i^{th} is the evaluated value of σ_i, σ_i^{exp} is the experimental value and N is the number of values. So χ^2 is the square of the deviation of the theoretical from the experimental values and the square root of χ^2 represents the average error in σ_i^{th} referred to σ^{exp}. The new parameters obtained by this step are:

$$V = 45.92 \text{ MeV} \qquad r_r = 1.22 \text{ fm} \qquad r_i = 1.298 \text{ fm}$$

All other parameters are unchanged in this step. The total cross-section evaluated with these parameters is plotted in Fig. 2 together with the KEDAK data.

The second step is to use the adjusted parameters by ABACUS in HAUSER*4/MOD and to vary some dominating parameters systematically.

This step is performed for two reasons:

i) The optimal parameters gained by ABACUS must not necessarily be the optimal parameters for use in HAUSER*4/MOD.
ii) It is of particular interest to see how σ_{tot} is sensitive to certain parameter variations.

The results from this sensitivity analysis can be seen from Fig. 3a to 3c. To discuss the results, we start with the variation of the real potential depth V. It is seen from Fig. 2 that the agreement to the KEDAK values in region below 100 keV is bad. This point is of particular interest and is discussed deeply in the following sect. 3.1.2. Nevertheless, if V is increased from 45.92 MeV to 47.01 MeV (the original Wilmore/Hodgson value) the agreement below 100 keV becomes better (see Fig. 3a), but above 100 keV σ_{tot} becomes too high. If on the other hand V is decreased to 45.0 MeV, σ_{tot} increases strongly below 100 keV simultaneously decreasing above 100 keV, however agreeing well with the KEDAK data in this region.

Now although V = 45.0 MeV gives good agreement above 100 keV, the values below 100 keV are much too high. It is therefore attempted to use the Wilmore/Hodgson value 47.01 MeV yielding for σ_{tot} relatively good agreement below 100 keV and to get better agreement above 100 keV by changing the real radius parameter r_r. This is shown in Fig. 3b. Decreasing r_r to 1.21 fm results in a satisfactory agreement above 100 keV, though σ_{tot} is slightly increased below 100 keV. A further decreasing of r_r to 1.20 fm on one hand gives better agreement above 100 keV but on the other hand σ_{tot} is increased too much below 100 keV.

From sect. 2.3 it follows that increasing V is compensated by decreasing r_r and vice versa. As it is clear from the variations in V_r and r_r described above, it is necessary to find a compromise in choosing the optimal values for V and r_r. So a high V value gives relatively good results above 100 keV but clearly the results below 100 keV are worse. On the other hand, a low value of V results in good agreement above 100 keV and a

high value of r_r gives good agreement below 100 keV. As can be seen from Fig. 3a and 3b to choose V = 47.01 MeV and r_r = 1.21 fm is a satisfactory compromise.

A further improvement is achieved by decreasing the imaginary potential depth W from 9.52 MeV to 9.0 MeV, thus σ_{tot} decreases slightly in the region 100 keV to ca. 1 MeV and slightly increases below the giant resonance near 4 MeV, while the region below 100 keV is nearly unaffected (see Fig. 3c). Comparing Fig. 3c and Fig. 2 it is obvious that choosing the parameters V = 47.01 MeV, r_r = 1.21 fm and W = 9.0 MeV instead of the ABACUS parameters results in equal agreement above 100 keV, whereas the results below 100 keV are improved. So the choice of the final parameters is justified:

$$
\begin{aligned}
&V = 47.01\ \text{MeV} - 0.267 \cdot E - 0.00118 \cdot \frac{E^2}{\text{MeV}} \\
&W = 9.0\ \text{MeV} - 0.53 \cdot E \qquad E \text{ in MeV} \\
&r_r = 1.21\ \text{fm} \qquad\qquad r_i = 1.298\ \text{fm} \\
&a_r = 0.66\ \text{fm} \qquad\qquad a_i = 0.48\ \text{fm}
\end{aligned}
\tag{3.2}
$$

With these parameters a χ^2 of $2.15 \cdot 10^{-3}$ was achieved, yielding an average deviation of the evaluated σ_{tot} values from the KEDAK data of ca. 5 %.

It should be noted that in contrast to the Wilmore/Hodgson parameters (2.27) the new adjusted parameters r_r and r_i are chosen to be mass independent. This is done because the nuclei considered here are close together and the mass dependence of the potential radii R_r and R_i, given by the $A^{1/3}$ law, is sufficient.

3.1.2 Discussion of the evaluated total cross-section

The σ_{tot} values of U-238 evaluated with the new adjusted parameters (3.2) are plotted in Fig. 4a together with the KEDAK-3 data. Above 50 keV the agreement is satisfactory over a wide region, only in the giant resonance region the experimental data are underestimated resulting from the use of

a spherical potential, for the deformation is strongest in this region /1/.

However, as mentioned in the previous section, there is a discrepancy in the region below 50 keV. So the KEDAK-3 value of σ_{tot} at 10 keV is ca. 13.7 barn, whereas the evaluated value is ca. 16 barn. From the previous section it is obvious that this discrepancy can only be solved by using a new set of parameters below 50 keV, for V, yielding good results below 50 keV, has to be increased by an amount which would destroy the good agreement above 50 keV. But it was the intention of this work to cover a wide energy region with one global set of parameters.

However there were some good reasons to suspect that the KEDAK data below 50 keV are too low:

i) The work of Madland and Young /1/ yielded σ_{tot} values for U-238 according to the results from this work using the global parameters (3.2). (see Fig. 1a).

ii) From Fig. 1a it can be seen that for nuclei with $232 \leq A \leq 239$ even the experimental data for σ_{tot} have the same tendency for 10 keV $\leq E \leq$ 50 keV as in the case of this work: with decreasing neutron energy σ_{tot} is increasing to reach a value near 16 barn at 10 keV. This behaviour of each nucleus is of course in agreement with the A-mass-dependent behaviour of σ_{tot} in the actinide region described in the introduction.

iii) Furthermore a literature search yielded the result that in the region 10 keV to 100 keV there are experimental σ_{tot} data of U-238 by Byoun and Block /30/. These data were higher than the KEDAK data.

Therefore a search was undertaken to see if the KEDAK data below 50 keV are correct, yielding, that raw instead of corrected transmission data were used for σ_{tot}. So the KEDAK-data below 50 keV were indeed too low.

Now at 10 keV the Byoun/Block value of σ_{tot} is ca. 14.8 barn, the value of this work evaluated using the parameters (3.2) is ca. 16 barn, so is the Madland/Young value, but the KEDAK value is ca. 13.7 barn. So the

evaluated σ_{tot}-value at 10 keV is still higher than the Byoun/Block value, the deviation however being smaller. Nevertheless, the new adjusted parameters being global parameters (3.2) were considered as suitable to reproduce optical model cross-sections in the region 10 keV to 15 MeV and to extrapolate to further transactinide nuclei: It must be kept in mind however that the cross-sections evaluated with the global parameters (3.2) are less accurate below 50 keV.

A further point confirming this σ_{tot}-evaluation was obtained by computing the s-wave strength function S_o. The strength function is a measure for the average width of the compound resonances per unit energy and is calculated in the resolved energy region from the ratio of the average neutron width $\bar{\Gamma}_{l,n}$ to the average resonance distance $\bar{D}$. The s-wave strength function can be extrapolated to the unresolved energy region by the following formula /2, 12/:

$$S_o = \frac{\bar{\Gamma}_{on}}{\bar{D}} = \frac{1}{2\pi} \cdot T_{l=o,n} \cdot \sqrt{\frac{1eV}{E}} \quad E \text{ in eV} \qquad (3.3)$$

Therefore S_o can be obtained by the s-wave optical model transmission coefficients $T_{l=o,n}$. The s-wave strength function calculated according to (3.3) from the optical model using the parameters (3.2) is $S_o = 1.18 \cdot 10^{-4}$, a value which is next to that calculated from the corrected Geel data giving $S_o = 1.14 \cdot 10^{-4}$ /31/ and also to the new ORNL value of $S_o = 1.168 \cdot 10^{-4}$ /46/, gained from the latest resonance data. In contrast, the KEDAK-3 value, gained by resonance analysis from experimental data in the resolved region, is $S_o = 1.02 \cdot 10^{-4}$ /31/.

3.1.3 Elastic Cross-Sections

In order to check further the evaluation performed, the elastic cross-section σ_{el} as well as the differential elastic cross-section is evaluated. To do this, first the compound elastic cross-section $\bar{\sigma}_{CE}$ is computed according to the Hauser/Feshbach formula (2.17) and following the semi-empirical method described in sect. 2.2b according to (2.18). The calculation of $\bar{\sigma}_{CE}$ according to (2.18) is done only in the case of U-238. Con-

cerning the other nuclei described in the following sections, there are no reliable σ_{ne}-data available.

From Fig. 5 it can be seen that up to ca. 1 MeV $\bar{\sigma}_{CE}$ obtained from both methods agrees relatively well. Above 1 MeV however, $\bar{\sigma}_{CE}$ calculated according to the Hauser/Feshbach formula decreases rapidly, $\bar{\sigma}_{CE}$ calculated with the semi-empirical method contributing an amount up to 7 MeV. This discrepancy is not analysed further, since $\bar{\sigma}_{CE}$ contributes not much compared to σ_{SE} in this region. Possible reasons are too low $\sigma_{n,e}$-data /27/ as an inadequate level density description according to Gilbert and Cameron.

In the further calculations, $\bar{\sigma}_{CE}$ obtained by the Hauser/Feshbach formula is used, since this method is also applicable for the other nuclei. The elastic cross-section obtained now by

$$\sigma_{el} = \sigma_{SE} + \bar{\sigma}_{CE}$$

agrees well with the KEDAK-3 data (cf. fig. 6) confirming the validity of $\bar{\sigma}_{CE}$.

For U-238 there are several experimental data of the elastic differential cross-section available /42-45/, so the possibility is given to check the quality of the optical model parameters used as well as that of the $\bar{\sigma}_{CE}$ evaluation performed. With the use of the subroutine DIFF implemented in HAUSER*4, $\frac{d\sigma_{SE}}{d\Omega}$ is computed according to eq. (2.31).

After this the differential compound elastic cross-section (2.19) being isotropic is added to $\frac{d\sigma_{SE}}{d\Omega}$ according to eq. (2.20). The results obtained in this manner are compared in Fig. 7a-h to experimental values. The agreement is excellent, confirming the choice of the optical model parameters (3.2) and the evaluation of $\bar{\sigma}_{CE}$ according to the Hauser/Feshbach formula.

3.2 Pu-240 and Pu-242 cross-sections

For Pu-240 and Pu-242 there are experimental σ_{tot}-data of Käppeler et al. /32/ in the range 10 keV to 400 keV, for Pu-240 there are additionally

data of Smith et al. /33/ for σ_{tot} and σ_{el} in the range 100 keV to 1.5 MeV. In the region 10 keV - 100 keV the Käppeler data however deviate nearly 35 % from measured σ_{tot}-data of U-238, being in contradiction to the assumed mass-dependent behaviour of σ_{tot} in the mass region $238 \leq A \leq 244$, as was shown in the introduction. So the σ_{tot}-value at 10 keV is for Pu-240 17.8 barn, for Pu-242 17.3 barn (Käppeler), however for U-238 this value is 13.7 barn (KEDAK-3) and 14.8 barn (Byoun and Block).

First an attempt was made to find optical model parameters being able to reproduce the Käppeler-data. In the case of Pu-242 it is not possible to find physically reasonable parameters giving satisfactory agreement of σ_{tot} with the Käppeler data. In the case of Pu-240 satisfactory agreement in the region 10 keV - 100 keV is achieved choosing the following parameters:

$$V = 45.0 \qquad W = 8.0 \qquad r_r = 1.20 \tag{3.5}$$

However, as is shown in the following, the parameters are hardly justified by physical arguments.

Assuming that the new adjusted parameters (3.2) reproduce σ_{tot} of U-238 satisfactory, being shown in sect. 3.1.1, there are two reasons for considering the parameters (3.5) as physically not justified: Firstly, going from U-238 to Pu-240 two nucleons are added, so the nuclear radius increases. According to (3.5) the real radius parameter is 1.20 fm, according to (3.2) r_r is 1.21 fm. So going from A = 238 to A = 240 by adopting the parameters (3.5) this would result in a smaller radius. Secondly, the potential depth V has to be mass-independent according to the Fermi gas model /e.g. 3/, adopting the parameters (3.5) would mean decreasing the potential depth from 47.01 MeV to 45.0 MeV.

A further reason not to use the parameters (3.5) is given by computing the s-wave strength function S_o according to eq. (3.3). Using the parameters (3.5) results in an extremely high value of $S_o = 1.7 \cdot 10^{-4}$. On the other hand, s-wave strength functions in the actinide region have values near $1.0 \cdot 10^{-4}$ according to the resonance analysis /31/ (cf. Tab. I). Using the parameters (3.2) adjusted to U-238 gives $S_o = 1.15 \cdot 10^{-4}$ for Pu-240 and

$S_o = 1.10 \cdot 10^{-4}$ for Pu-242. These are values near to those from the resonance analysis.

The reflections on the A-dependence of σ_{tot} in the range $238 \leq A \leq 244$ (cf. introduction and sect. 3.1.2) furthermore show that σ_{tot} should have a value between 15 and 16 barn at 10 keV, being achieved by using the parameters (3.2) adjusted to U-238. As can be seen from Fig. 8, the σ_{tot}-values of U-238, Pu-240 and Pu-242, being evaluated with the parameters (3.2) which are considered to be valid, lie close together and furthermore they are close to the experimental U-238 data of Byoun and Block, whereas the Pu-240 and Pu-242 data of Käppeler are extremely high.

From the evaluations and reflections described above the conclusion has to be drawn that the parameters (3.2) adjusted to U-238 are able to reproduce neutron cross-sections satisfactorily for $A \geq 238$ in the range $10 \text{ keV} \leq E \leq 15 \text{ MeV}$, whereas the data of Käppeler appear to be too high in the interval 10 keV to 100 keV.

After computing the compound elastic cross-section with the Hauser/Feshbach formula the elastic cross-section is computed for the isotopes Pu-240 and Pu-242. The values obtained for the total and elastic cross-sections are shown in Fig. 9 - 10 together with the available experimental data.

3.3 Am-241 and Cm-244 cross-sections

Originally it was intended to evaluate only optical model cross-sections for the even-even nuclei U-238, Pu-240, Pu-242 and Cm-244. In a later stage of the work it was decided to consider additionally the capture cross-section and, as the capture cross-section of Am-241 is of particular interest, the cross-sections for the odd-even nucleus Am-241 were also taken into account.

Based on the A-systematics the parameters (3.2) adjusted to U-238 are used to compute σ_{tot} of Am-241 and Cm-244. Especially in the case of Cm-244 a set of parameters, being able to extrapolate, is necessary, for no experimental σ_{tot}-data of Cm-244 exist.

There are however several evaluations for Cm-244 /34/ showing large discrepancies. The present evaluated σ_{tot}-data are compared with those evaluations in Fig. 14. The present evaluation is considered to be valid because of its systematic A-dependence. It is satisfactory that the present evaluation lies approximately in the middle of the other evaluations. From Fig. 12, where the evaluated total cross-sections for all nuclei considered here are plotted, the systematic A-dependence of σ_{tot}, cited several times, is obvious.

In the case of Am-241 there are experimental σ_{tot}-data of Phillips and Howe /35/ in the range 3 - 20 MeV. These data are confirmed excellently by this evaluation. Here the validity of the parameters (3.2) to reproduce total cross-sections for $A \geq 238$ is evident at least for $E \geq 3$ MeV.

The elastic cross-sections for Am-241 and Cm-244, obtained according to the procedure described in sect. 3.2, are plotted in Fig. 11b and 13b. There are, however, no experimental σ_{el}-data.

3.4 Computing the capture cross-sections

The capture cross-section $\sigma_{n,\gamma}$ is calculated with the Hauser/Feshbach formula using the formalism described in sect. 2.6 to obtain the capture transmission coefficients. The level density is represented by the 'constant temperature formula' as well as the 'Fermi gas formula'. The density parameters are computed following the semi-empirical formulae according to Gilbert and Cameron described in sect. 2.6 and they are listed in tab. II.

For U-238 there are experimental $\sigma_{n,\gamma}$-data in the range 10 keV to 10 MeV, for Pu-240, Pu-242 and Am-241 in the range 10 keV to ca. 300 keV /27, 36 - 39/. These data are processed in the nuclear data file KEDAK-3 /27, 40/. Therefore it is tried to reproduce the KEDAK-3 capture data for the nuclei mentioned above. In the case of Cm-244 there are no experimental $\sigma_{n,\gamma}$-data, only several evaluations exist.

As a starting point of the capture cross-section evaluation, the Holmes/ Woosley values for the parameters K_E, K_M, Γ_{GDR} and ε_{GDR}, given in sect. 2.6,

are used and also the density parameters according to Gilbert and Cameron, given in Tab. II. However, using these parameters, the agreement in $\sigma_{n,\gamma}$ to the KEDAK-3 data is unsatisfactory. So it is tried to improve the agreement by adjusting the empirical constants K_E and K_M.

$\sigma_{n,\gamma}$ is hardly sensitive on changing K_M, therefore in the further evaluation the Holmes/Woosley value $K_M = 0.005$ is used, on changing K_E, however, $\sigma_{n,\gamma}$ is very sensitive. The optimal adjusted K_E-values are listed in Tab. II for the specific compound nuclei.

As can be seen from Fig. 15 - 17, the $\sigma_{n,\gamma}$-values, evaluated with these parameters, agree relatively well with the KEDAK-3 data. In the case of U-238, where the experimental $\sigma_{n,\gamma}$-data reach up to 10 MeV, it is shown that the representation of the level density according to Gilbert and Cameron is sufficient to reproduce capture cross-sections above 1 MeV. Concerning the other nuclei, the experimental data reaching only up to ca. 300 keV, the capture cross-section above 300 keV is less well established. It is assumed however, that it is relatively accurate as in the case of U-238.

In the case of Cm-244, where no measured $\sigma_{n,\gamma}$-data exist, the K_E-value 1.25 is used. From Fig. 20 it is seen that the present evaluation of $\sigma_{n,\gamma}$ agrees well with the other evaluations, whereas in the case of σ_{tot} there are large discrepancies, as mentioned above.

Below the inelastic threshold, the possibility is given by the optical model to compute the capture cross-section $\sigma_{n,\gamma}$ by subtracting the compound elastic cross-section from the absorption cross-section σ_{abs}. The reaction cross-section σ_r obtained by doing this subtraction agrees with the capture cross-section below the inelastic threshold since no further reactions take place in this energy range besides the sub-threshold fission, which can be neglected.

The reaction cross-sections evaluated are plotted in Fig. 15b - 19b together with the KEDAK capture cross-sections. It is seen that the reaction cross-sections evaluated reproduce indeed the capture data below the inelastic threshold, lying between 40 and 50 keV for the nuclei considered.

Considering the progress of the reaction cross-section, the opening of the inelastic channels becomes obvious. σ_r, being given by $\sigma_{n,\gamma}$ below the inelastic threshold and therefore decreasing with increasing energy, decreases spasmodically when reaching the inelastic threshold. In this region the main part of σ_r is given by the inelastic scattering, whereas the fission becomes significant above 1 - 2 MeV.

4. Conclusion

Optical model cross-sections, especially σ_{tot}, show a systematic A-dependence in the unresolved energy region and therefore should be evaluated under this aspect, however being often ignored in the past. Cross-section evaluations for individual nuclei without taking into account A-systematics, often yield discrepant results, especially if nuclei are considered for which no experimental data exist. This was demonstrated in the case of Cm-244. Measuring total cross-sections, an analysis should be made to see if the measured data are consistent with the A-systematics.

The spherical optical model now being used for over 20 years was shown to be still the evaluator's most useful tool to obtain theoretically cross-sections in the unresolved energy region. Furthermore it was shown, that the optical model is even able to criticize discrepant experimental data, which was demonstrated in the case of the inconsistent experimental σ_{tot}-data of Pu-240, Pu-242 and U-238.

The present work shows that a spherical potential is sufficient to obtain average neutron cross-sections in a satisfactory manner, even in the case of strongly deformed nuclei. A spherical potential, being approximately equally efficient, needs much less computing time than a deformed potential, since there the Schrödinger equation cannot be separated into partial waves, leading to a system of coupled differential equations. As long as no inelastic processes are considered, it seems to be sufficient to evaluate optical model cross-sections with a spherical potential. This can also be deduced from the work of Madland and Young /1/ (cf. Fig. 1a and 1b).

Capture cross-sections can be obtained by adjusting with the simple giant dipole resonance model. The evaluated capture data of U-238 show that the continuum is well represented by a level density according to Gilbert and Cameron. Further capture cross-section measurements in the future will be necessary to check the evaluated capture data above 300 keV for the other nuclei considered here.

Finally the optical model calculation was confirmed by computing the differential elastic cross-section of U-238 showing excellent agreement with experimental data. Furthermore, this shows that angle distributions can be obtained satisfactorily, even neglecting the spin in the scattering process.

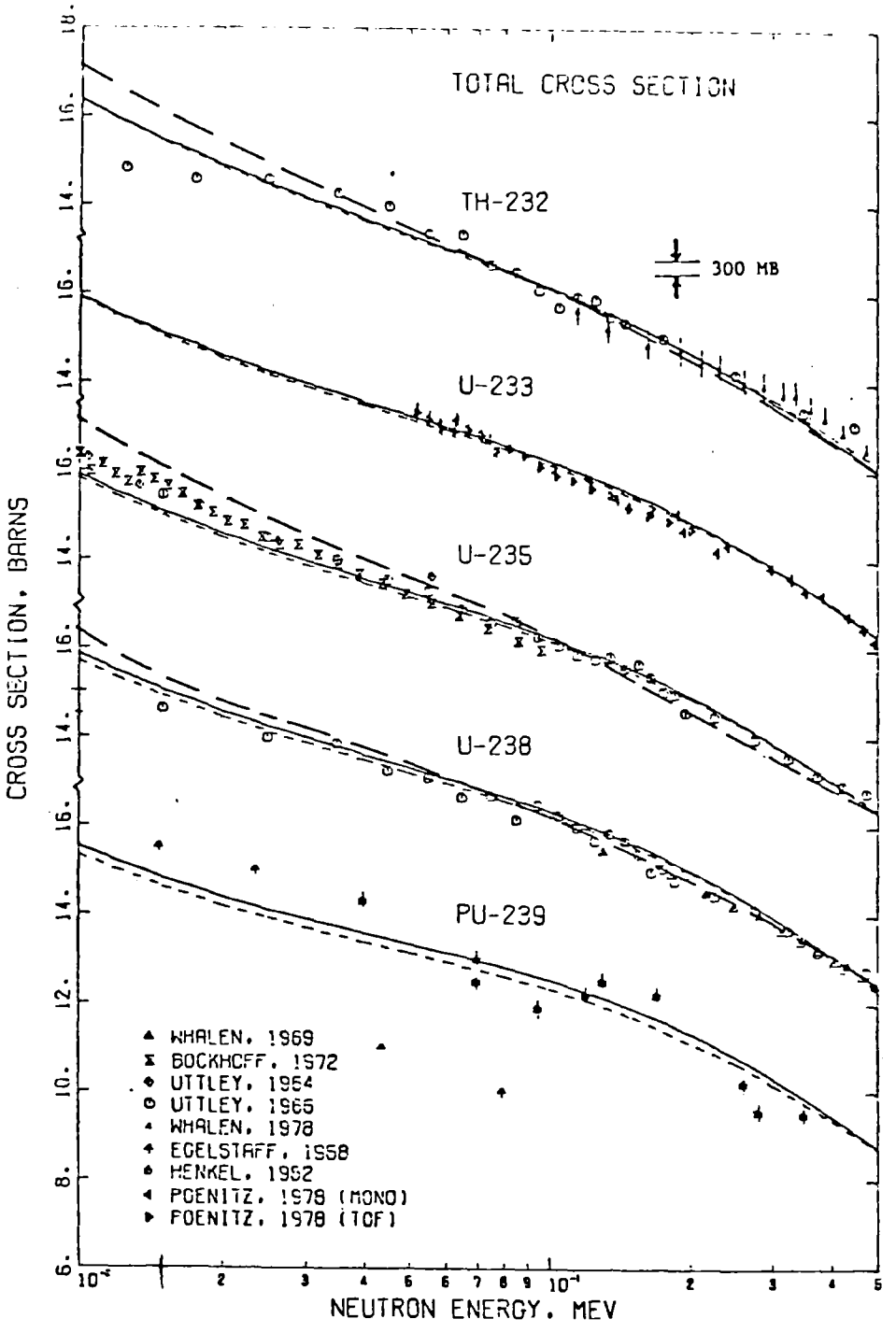

Fig. 1a Total cross-sections for some actinide nuclei evaluated by Madland and Young /1/

------- spherical optical model

——— improved form of the spherical model (cf. /1/)

—— —— deformed optical potential

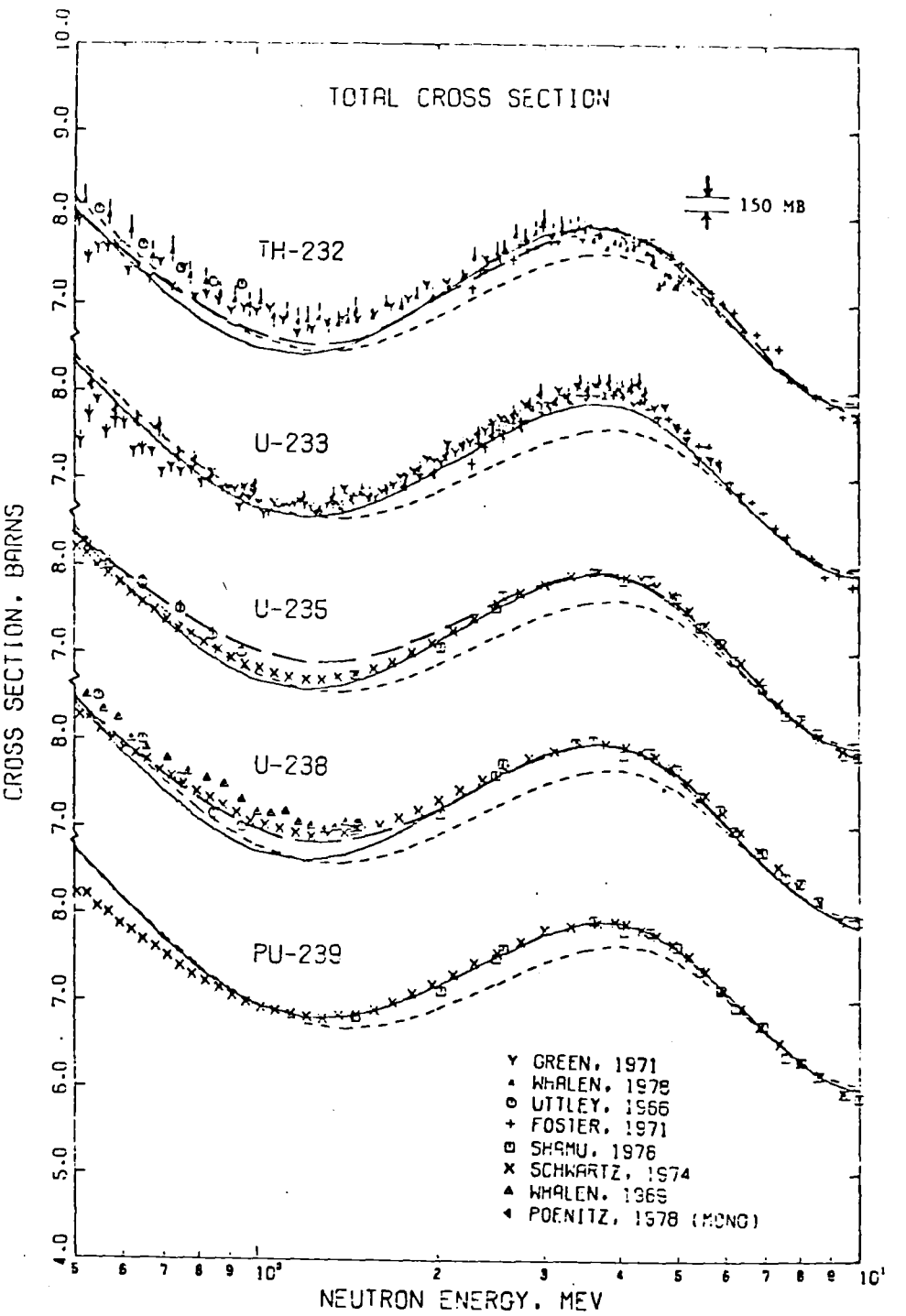

Fig. 1b **Total cross-sections for some actinide nuclei evaluated by Madland and Young /1/**

------- **spherical optical model**

——— **improved form of the spherical model (cf. /1/)**

— — **deformed optical potential**

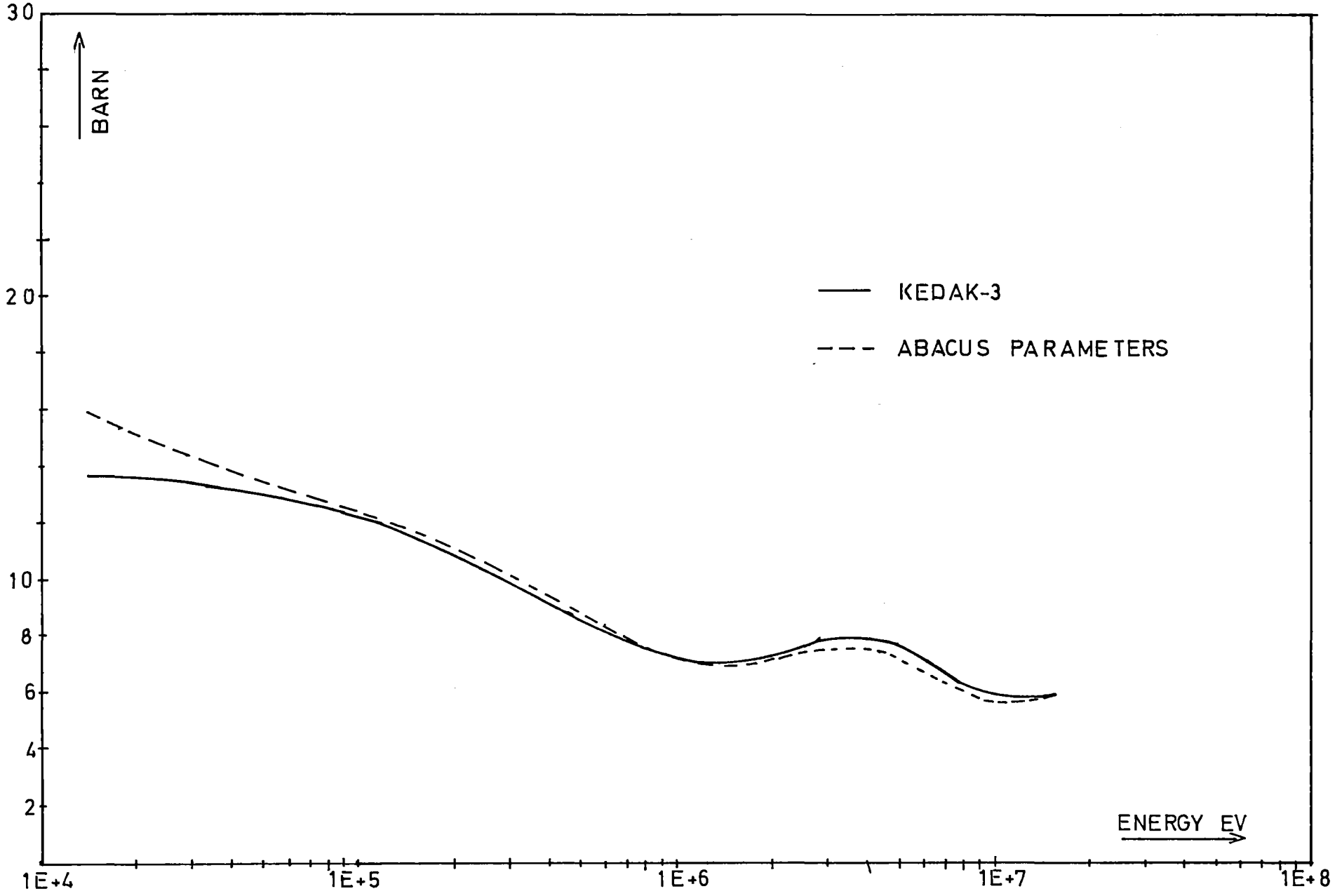

Fig. 2 Total cross-section of U-238 calculated with the ABACUS-parameters

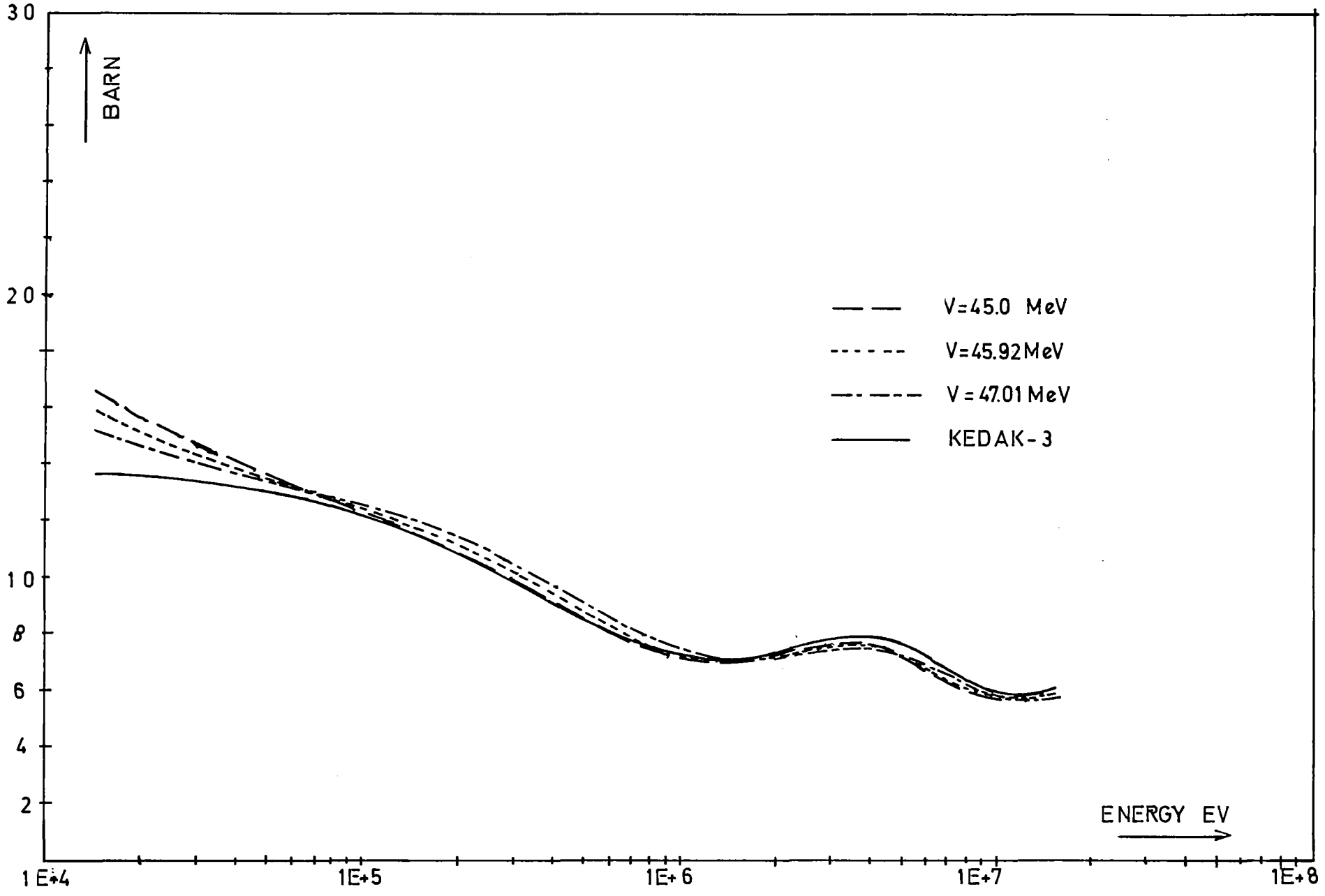

Fig. 3a Evaluated total cross-section of U-238 at several real potential depths

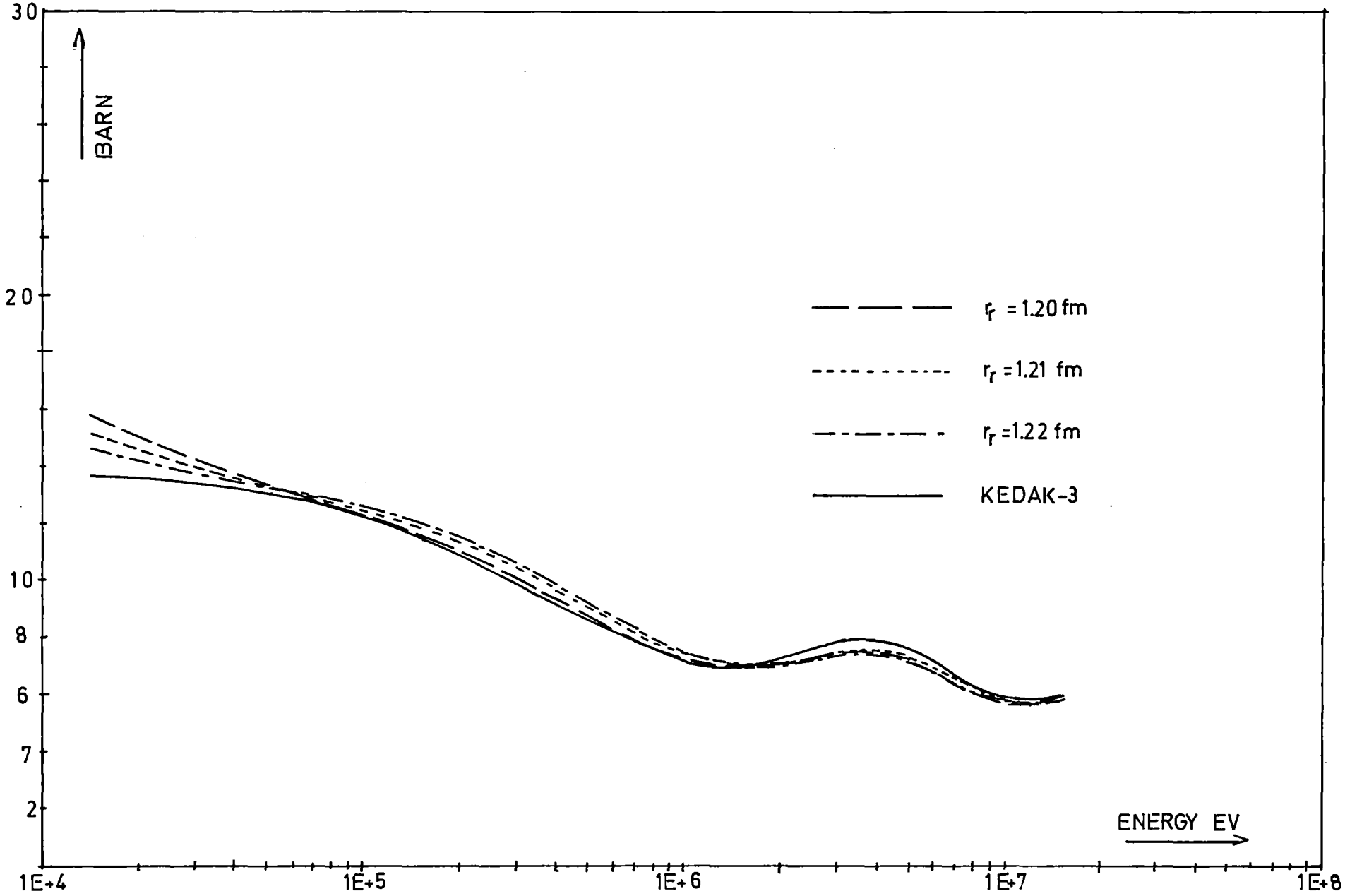

Fig. 3b Evaluated total cross-section of U-238 with V_r = 47.01 MeV at several real radii

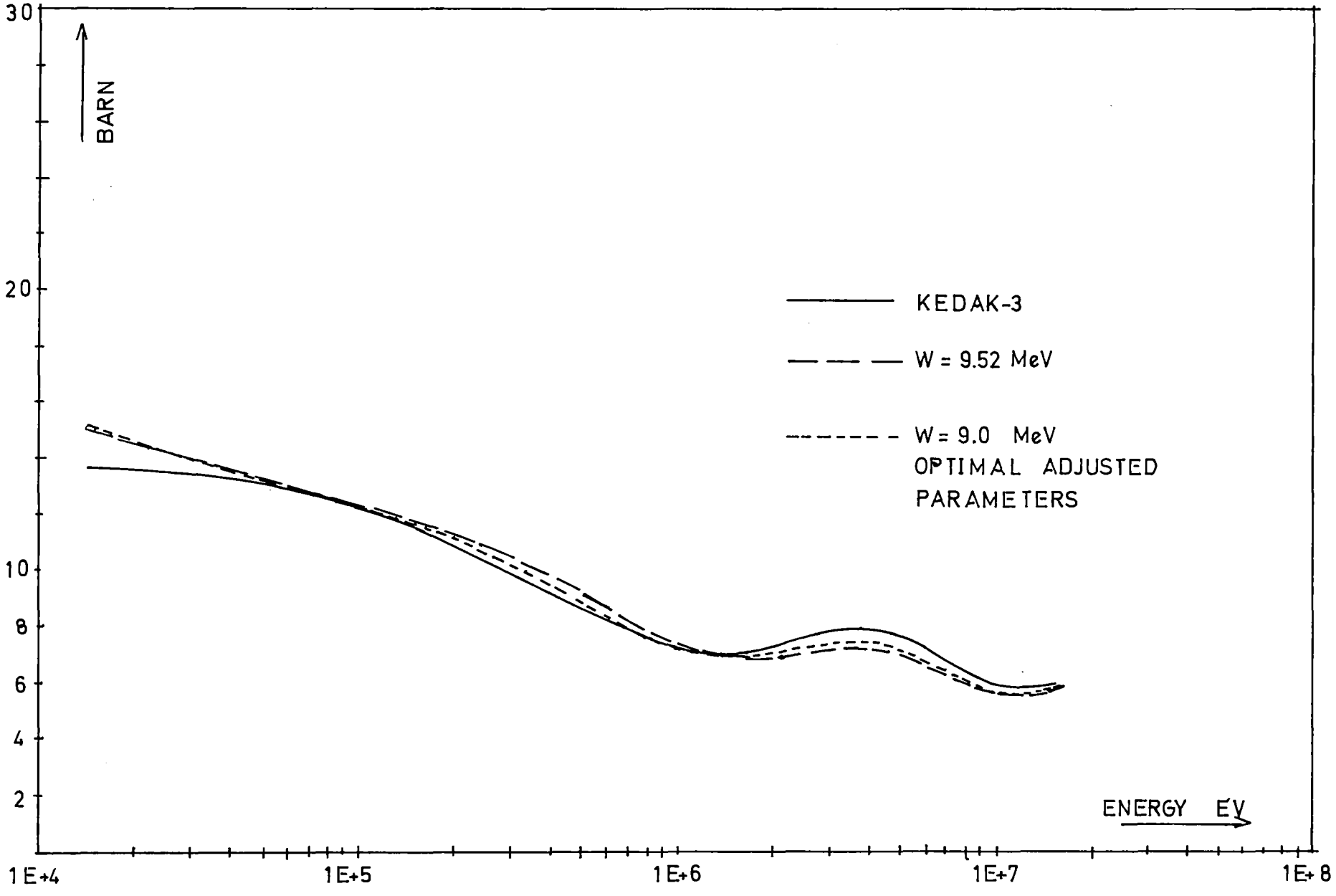

Fig. 3c Evaluated total cross-section of U-238 with V_r = 47.01 MeV and r_r = 1.21 fm

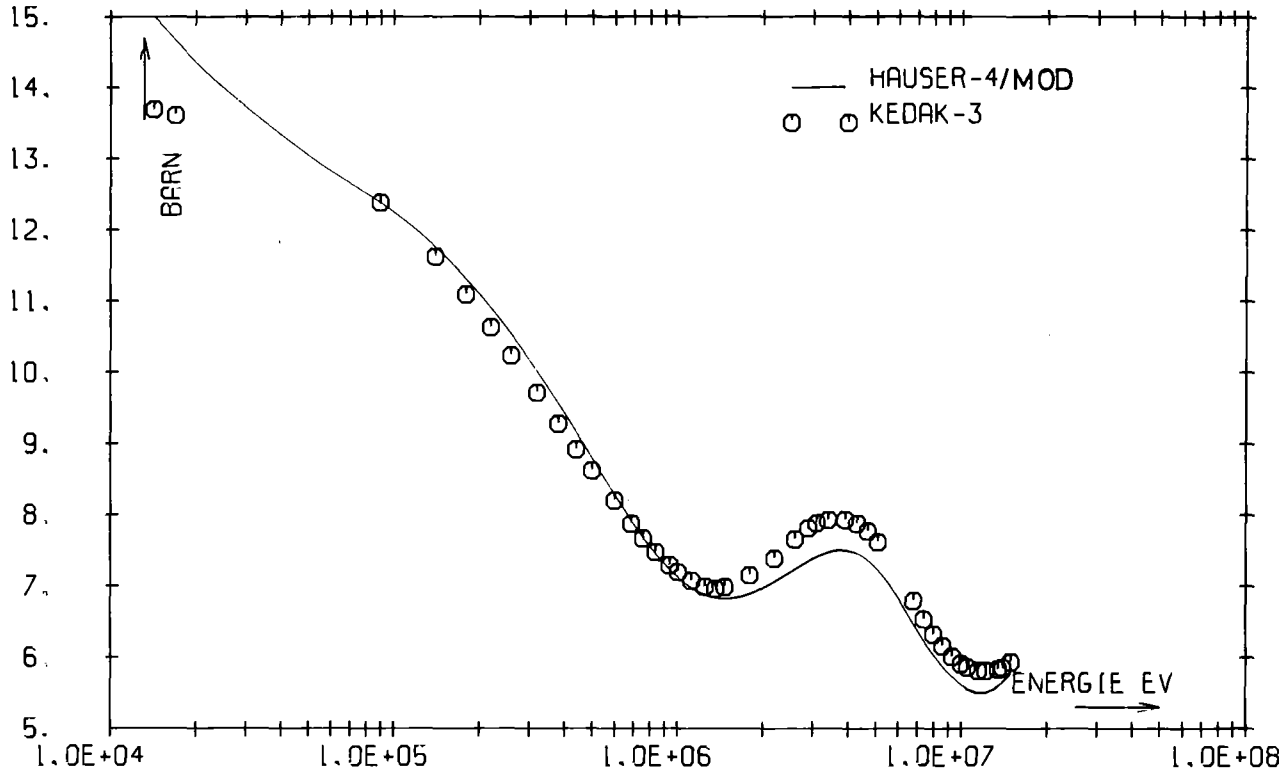

Fig. 4a Evaluated and KEDAK-3 total cross-section of U-238

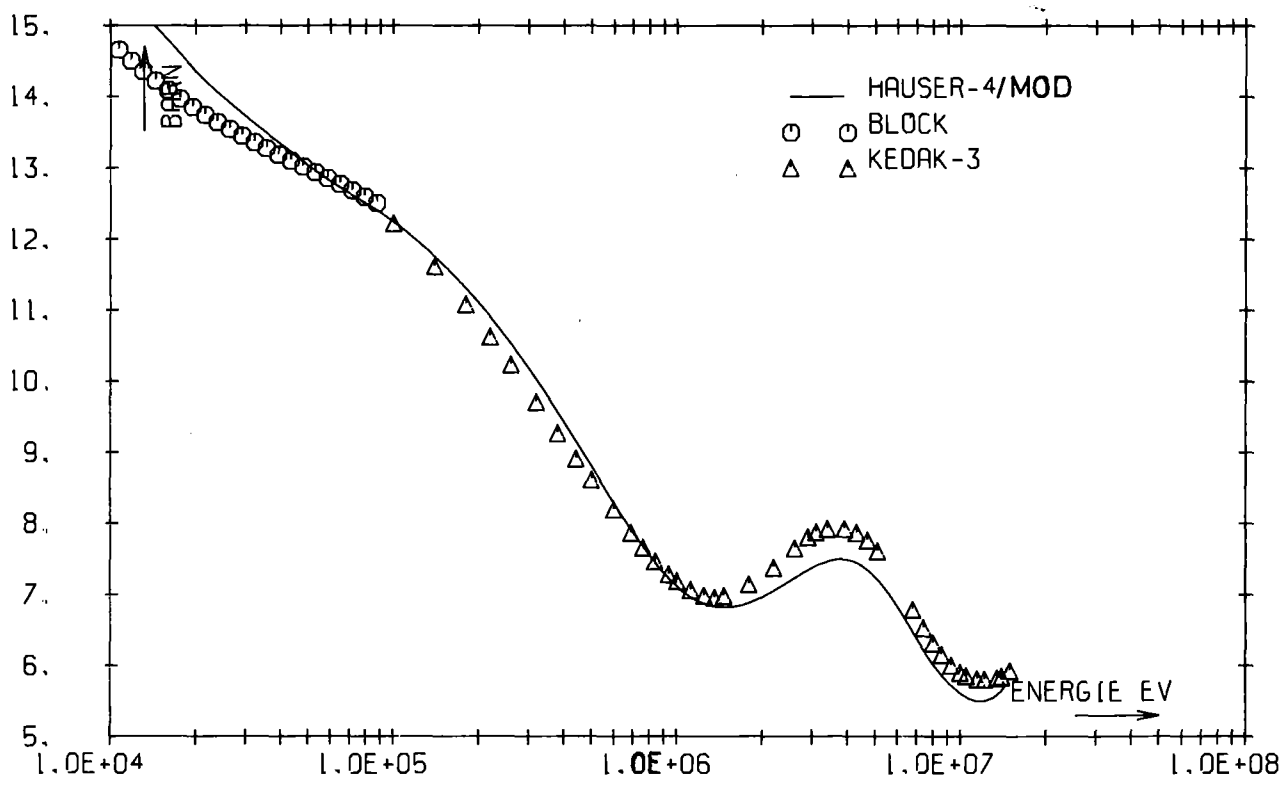

Fig. 4b Evaluated and measured total cross-section of U-238

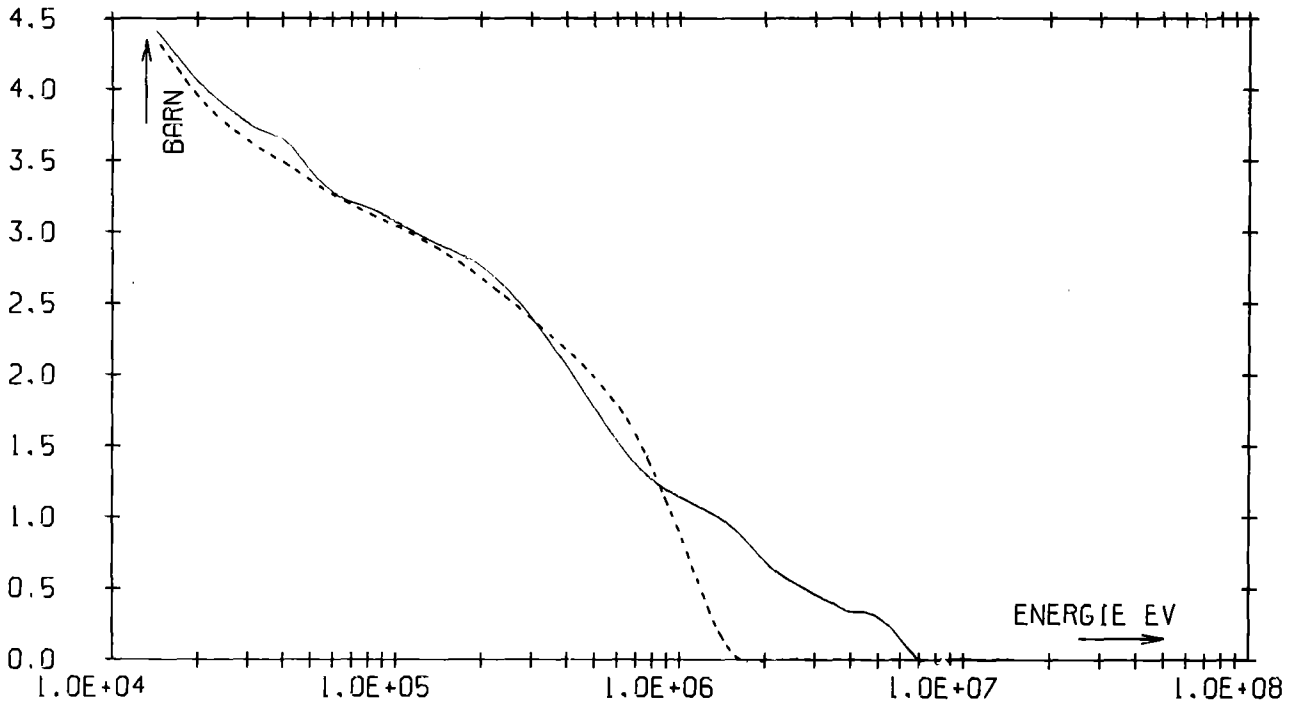

Fig. 5 Compound-elastic cross-section of U-238

—— **evaluated with the semi-empirical method**

---- **evaluated according to the Hauser/Feshbach formula**

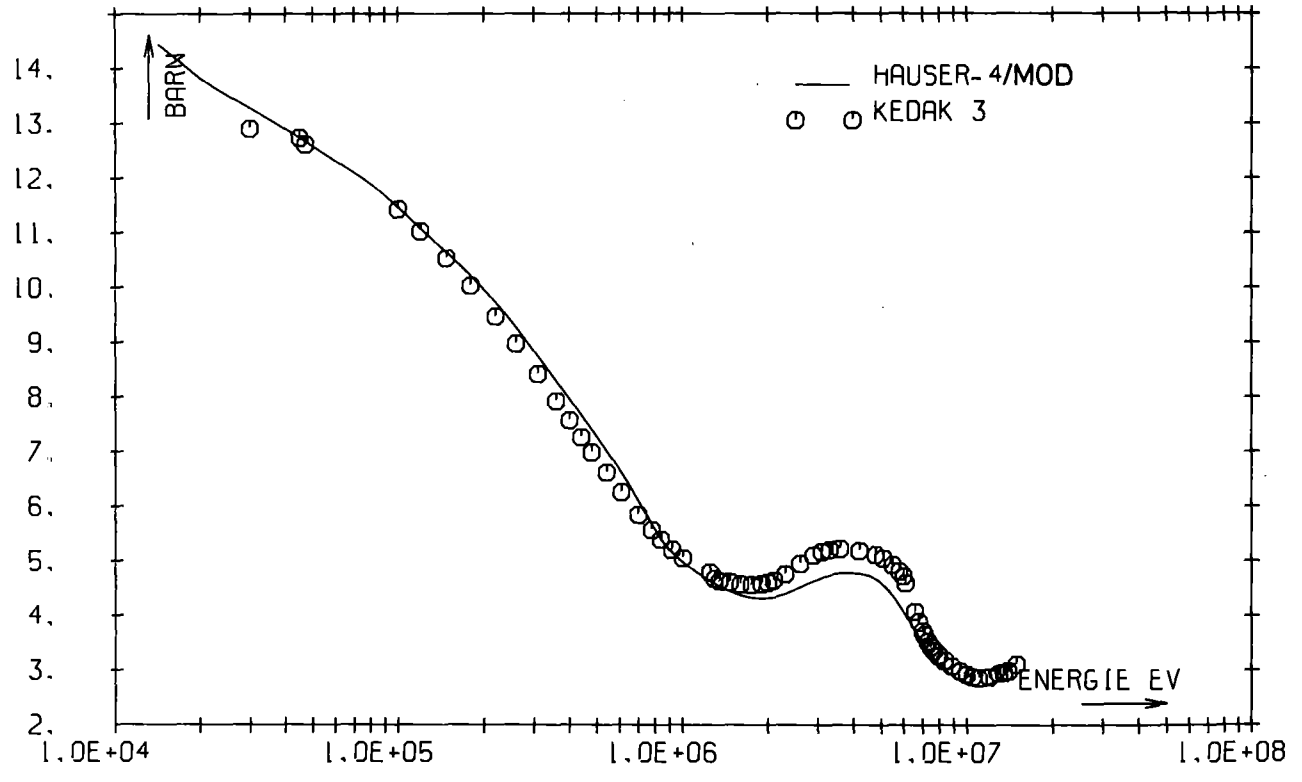

Fig. 6 U-238 Elastic cross-section

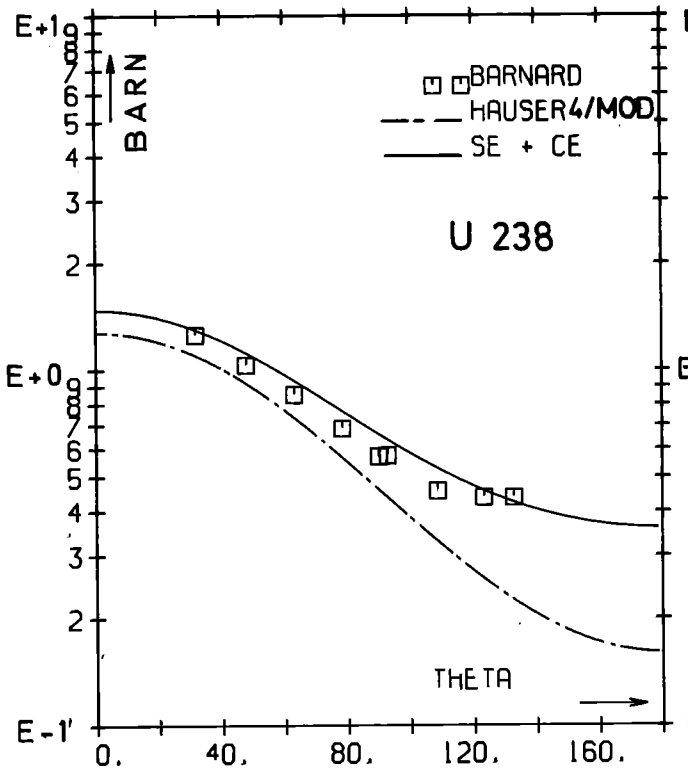

Fig. 7a E=0.25 MeV

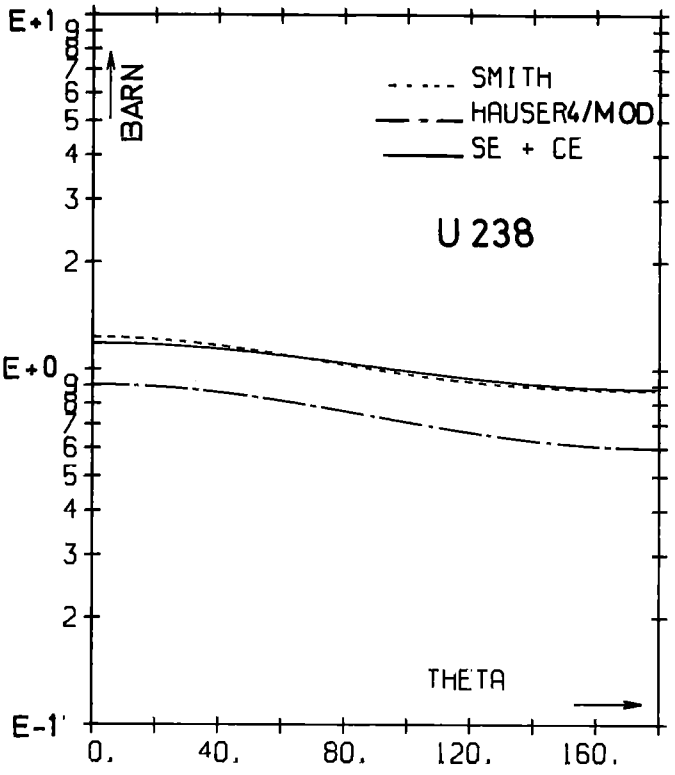

Fig. 7b E=0.045 MeV

The curves signed with HAUSER4/MOD show the differential shape-elastic cross-section, those signed with SE+CE the total differential elastic cross-sections.

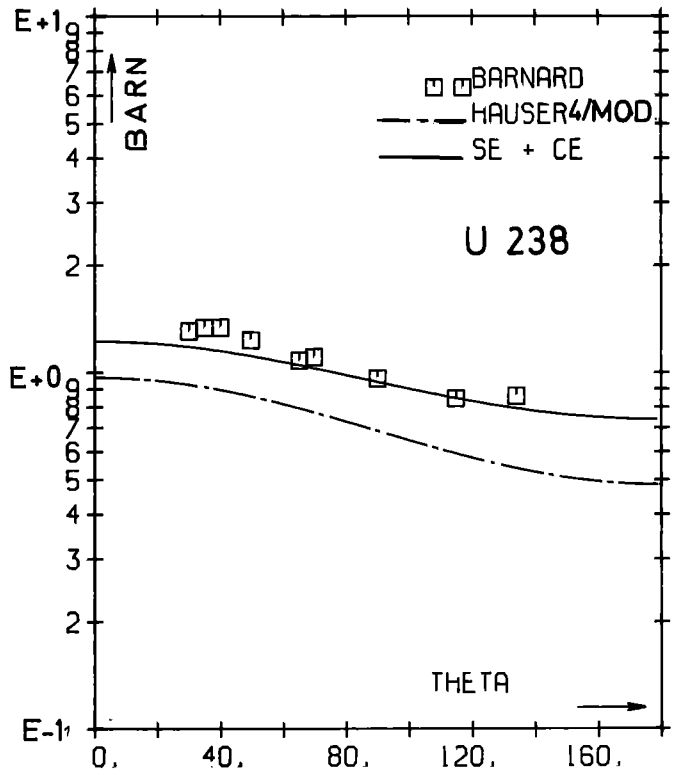

Fig. 7c E=0.075 MeV

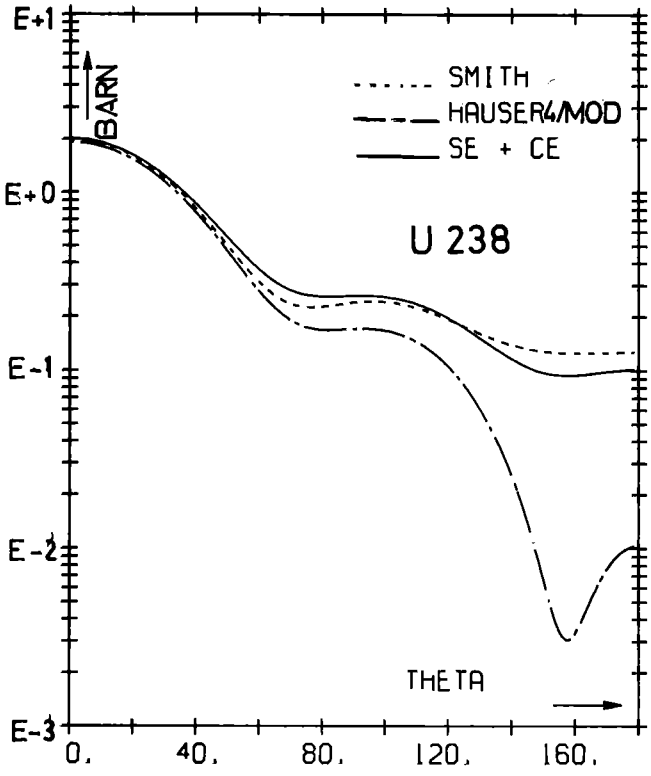

Fig. 7d E=1.0 MeV

Fig. 7a-d Differential elastic cross-section of U-238

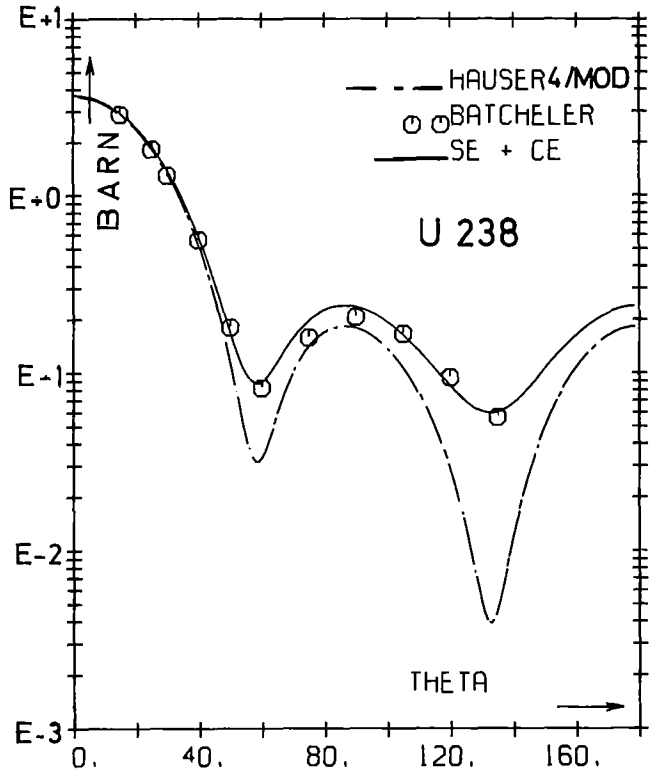

Fig. 7e E=2.0 MeV

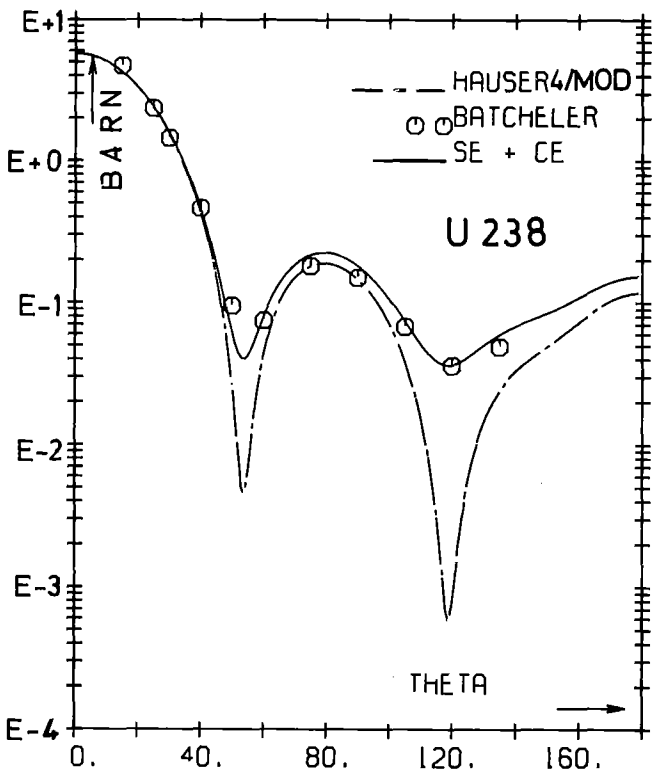

Fig. 7f E=3.0 MeV

The curves signed with HAUSER4/MOD show the differential shape-elastic cross-section, those signed with SE+CE the total differential elastic cross-sections.

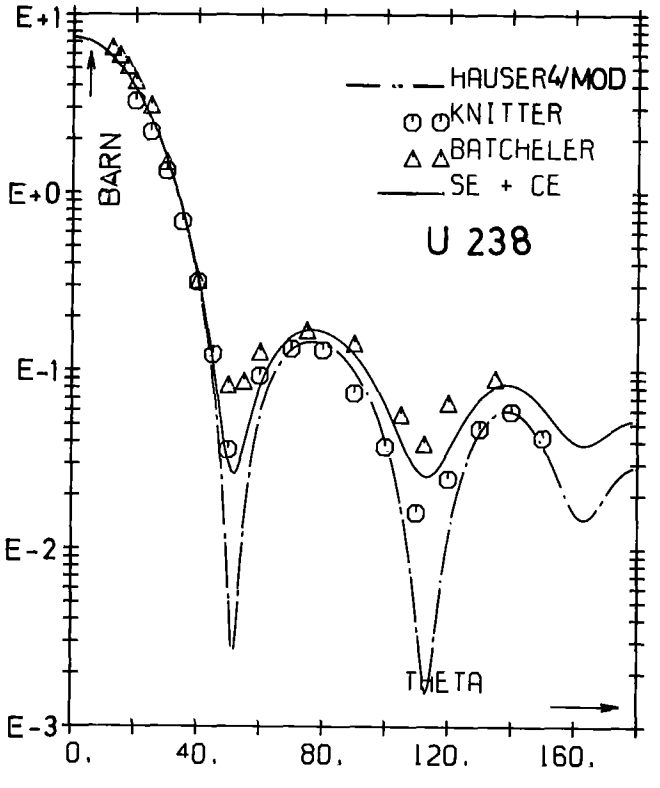

Fig. 7g E=4.0 MeV

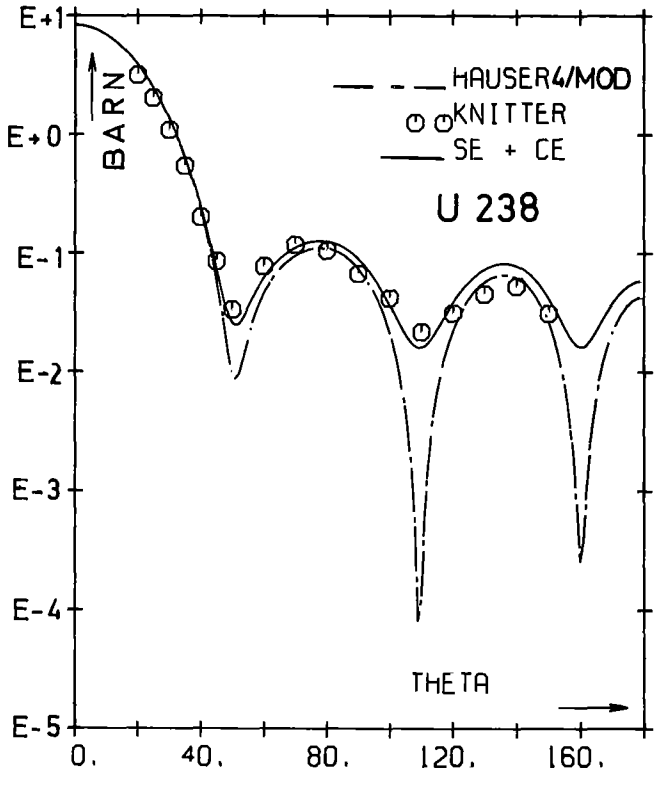

Fig. 7h E=5.0 MeV

Fig. 7e-h Differential elastic cross-section of U-238

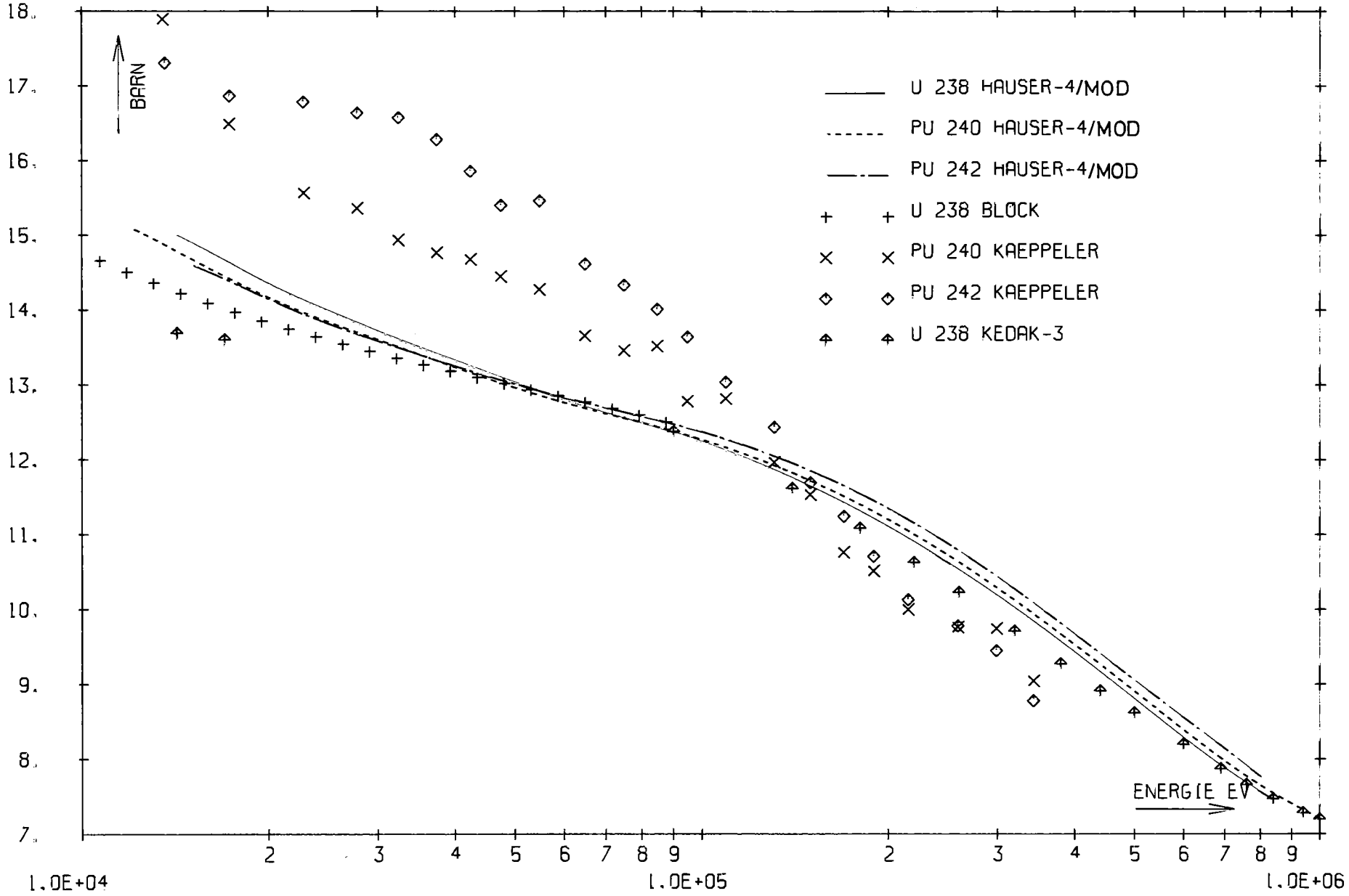

Fig. 8 Evaluated and measured total cross-sections for the nuclei U-238, Pu-240 and Pu-242 in the range 10 keV to 1 MeV

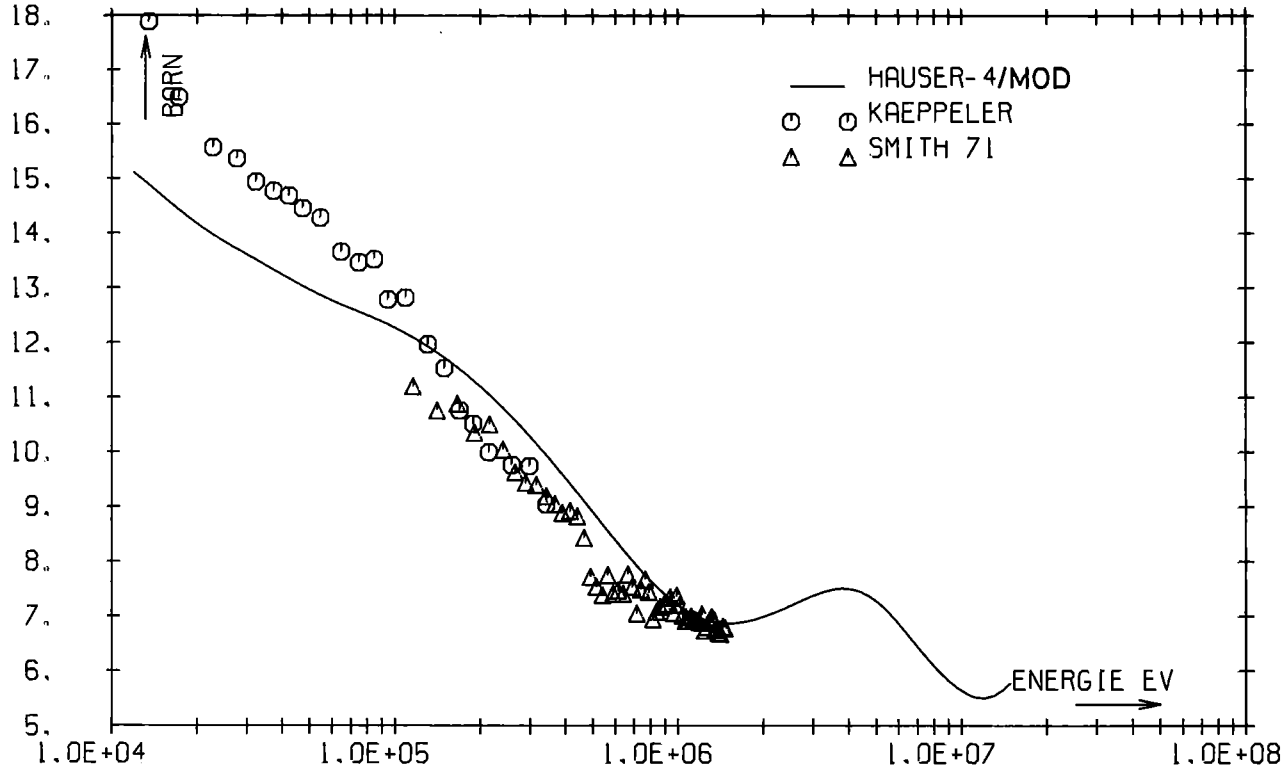

Fig. 9a Pu-240 Total cross-section

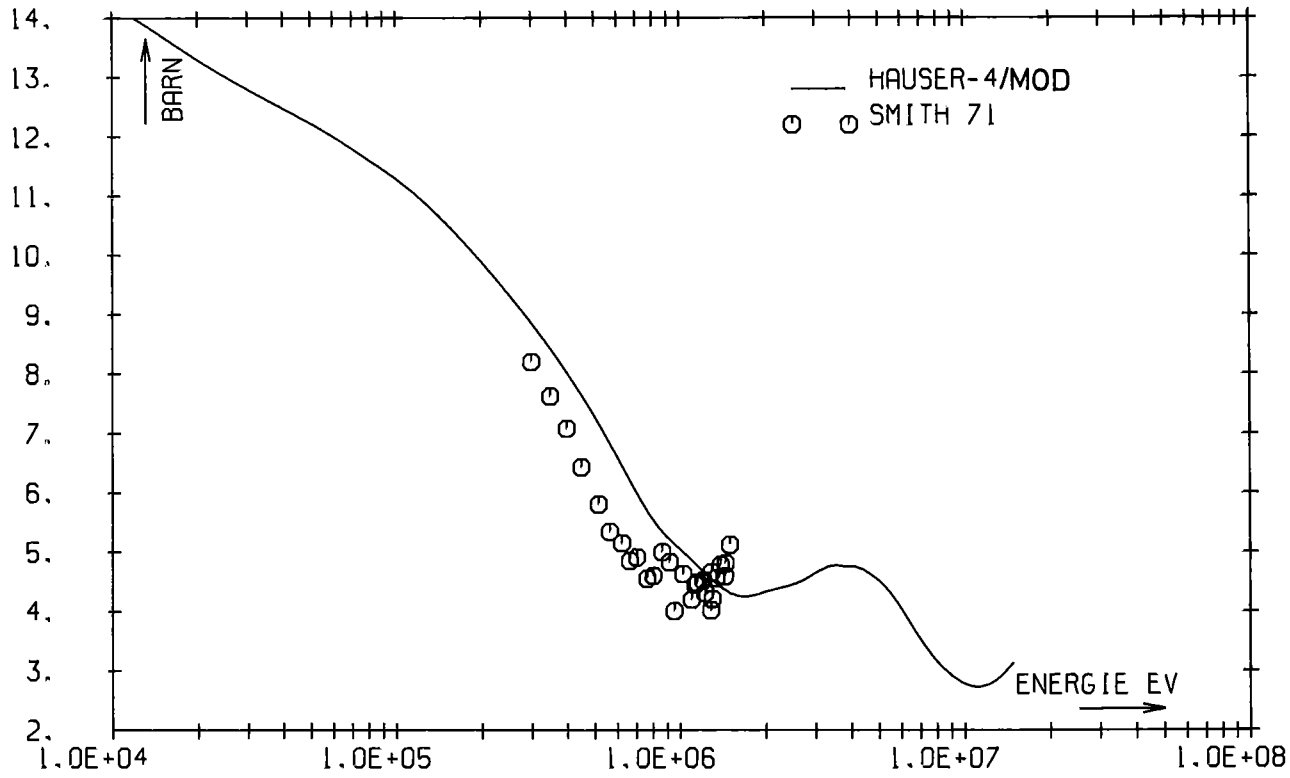

Fig. 9b Pu-240 Elastic cross-section

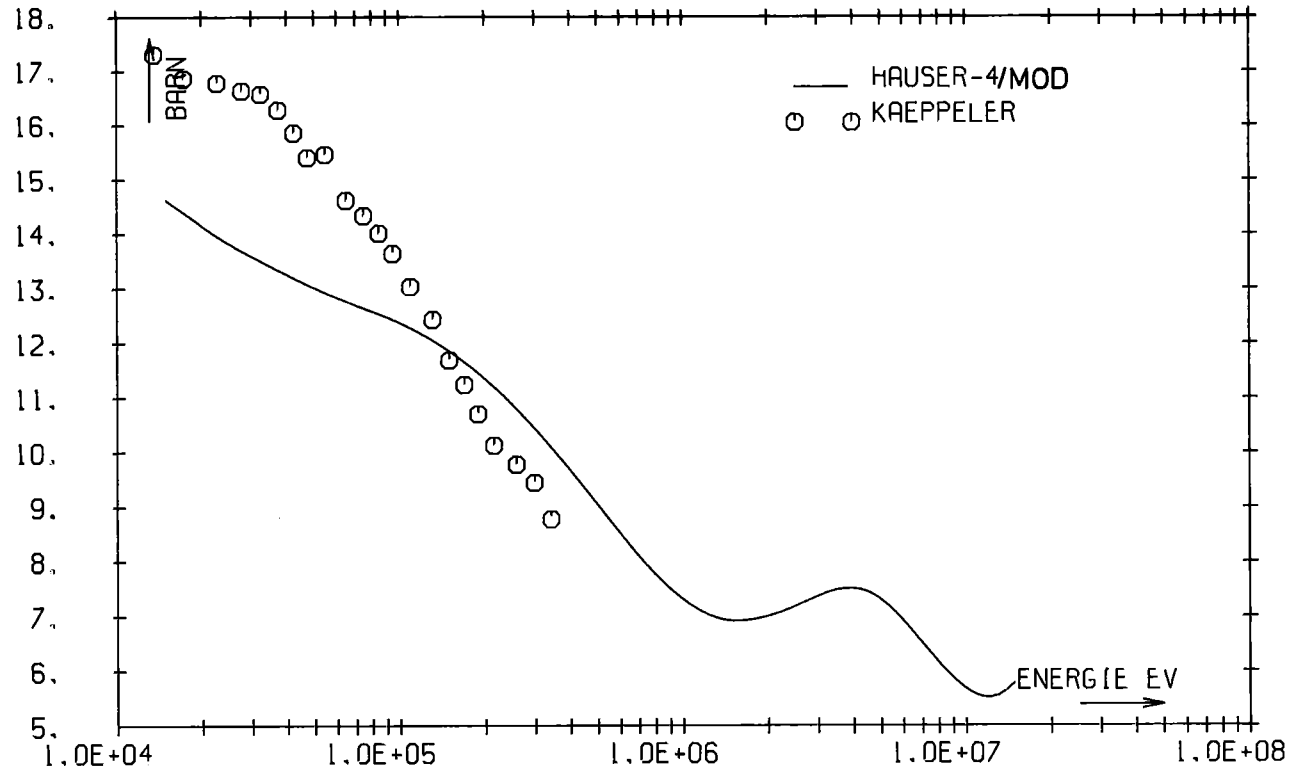

Fig. 10a Pu-242 Total cross-section

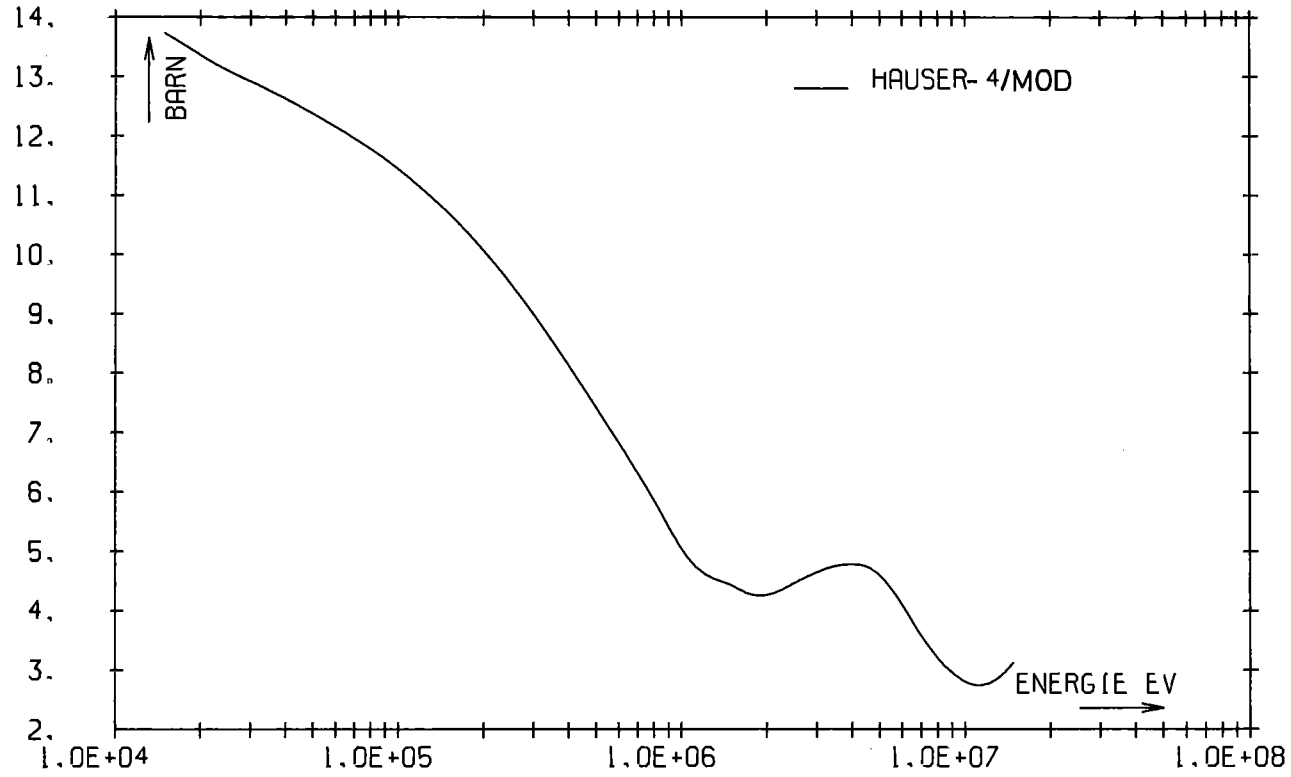

Fig. 10b Pu-242 Elastic cross-section

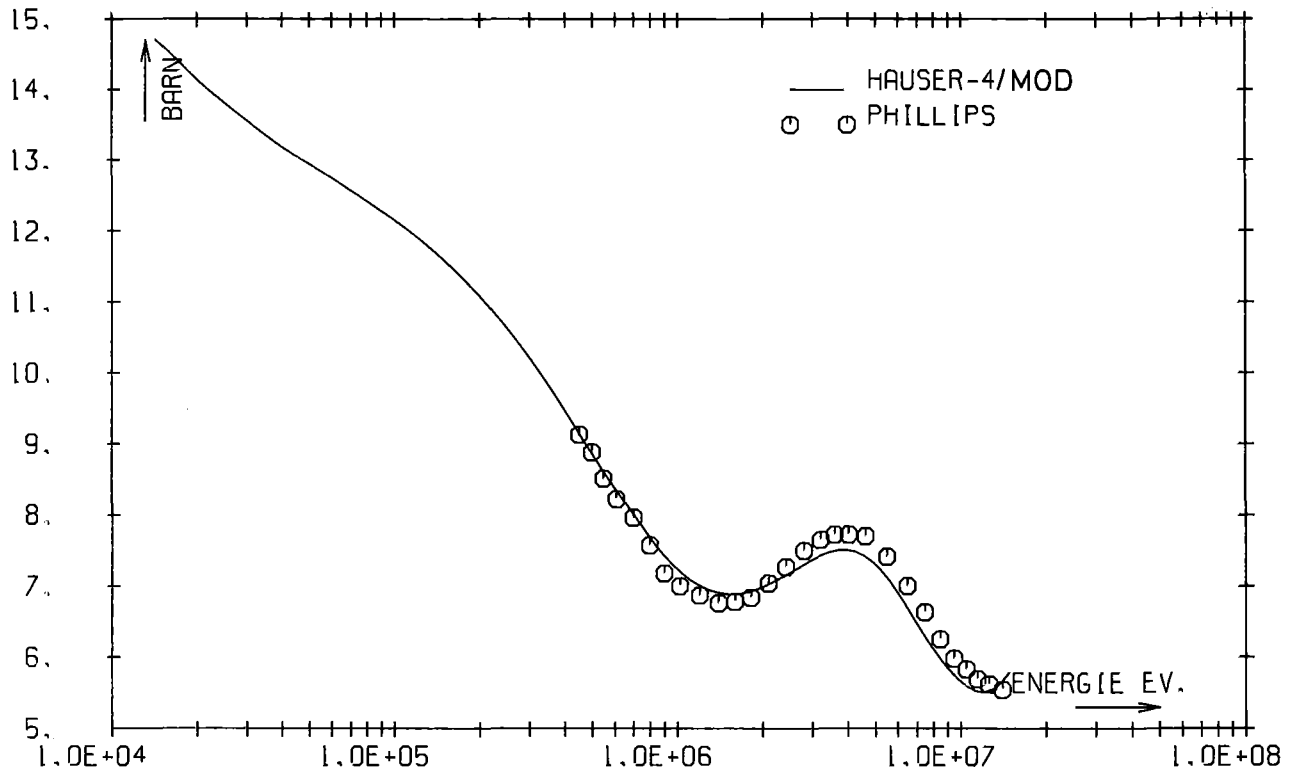

Fig. 11a Am-241 Total cross-section

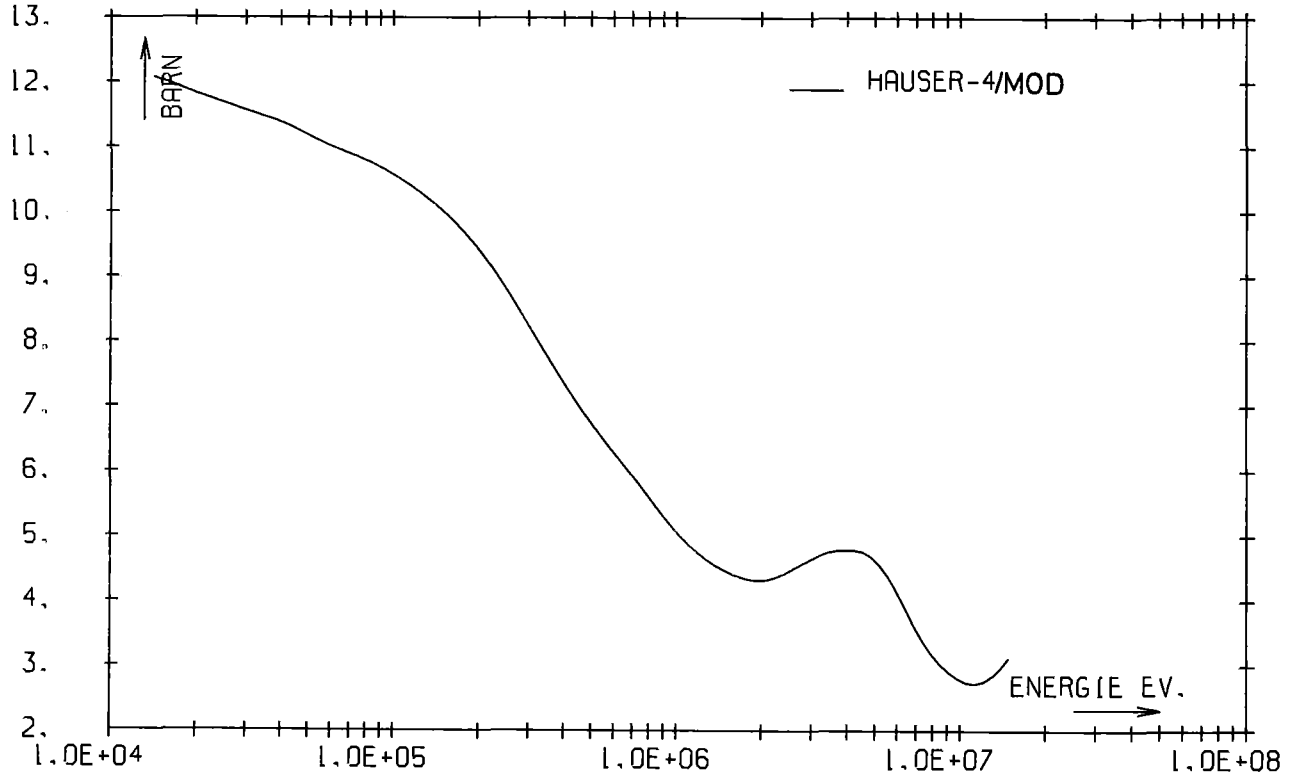

Fig. 11b Am-241 Elastic cross-section

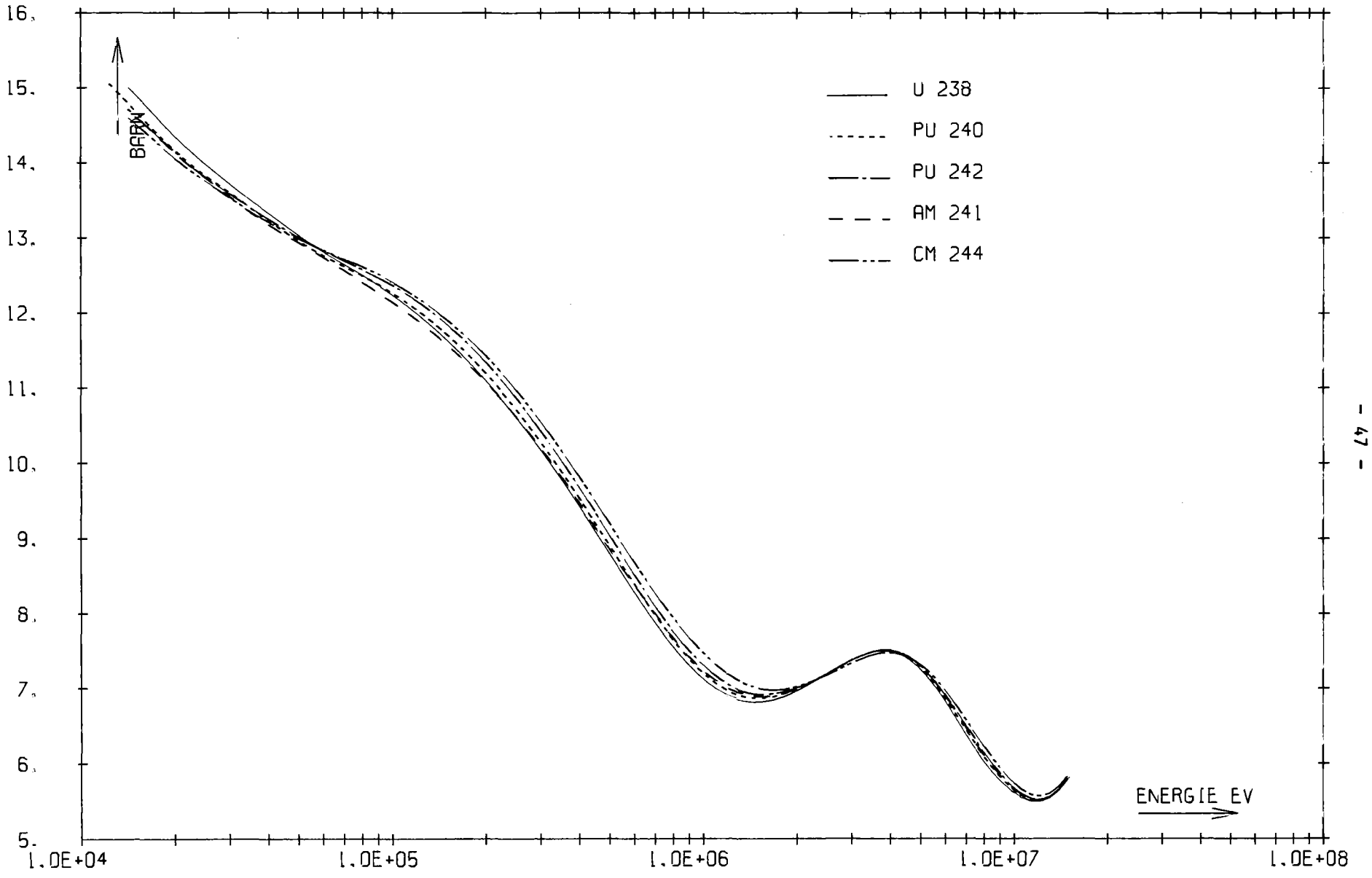

Fig. 12 Evaluated total cross-sections for the nuclei U-238, Pu-240, Pu-242, Am-241 and Cm-244 in the range 10 keV to 15 MeV

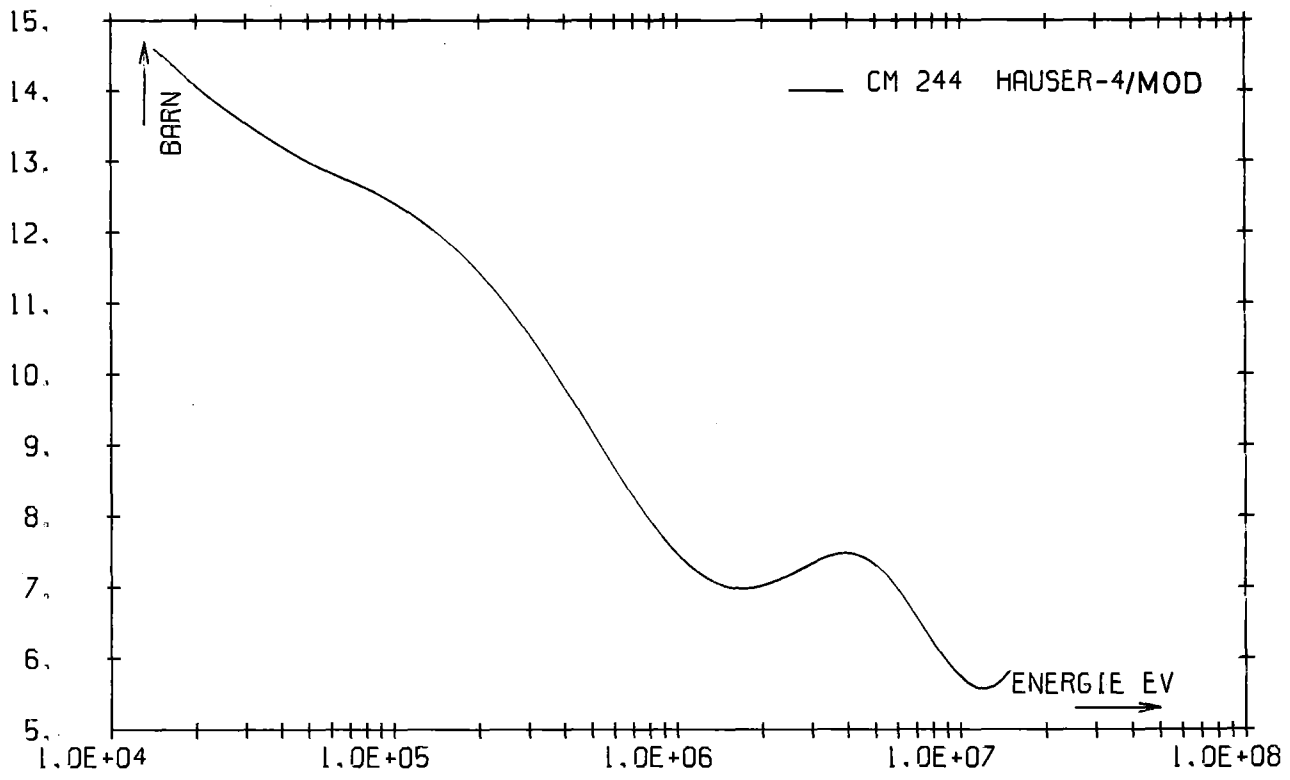

Fig. 13a Cm-244 Total cross-section

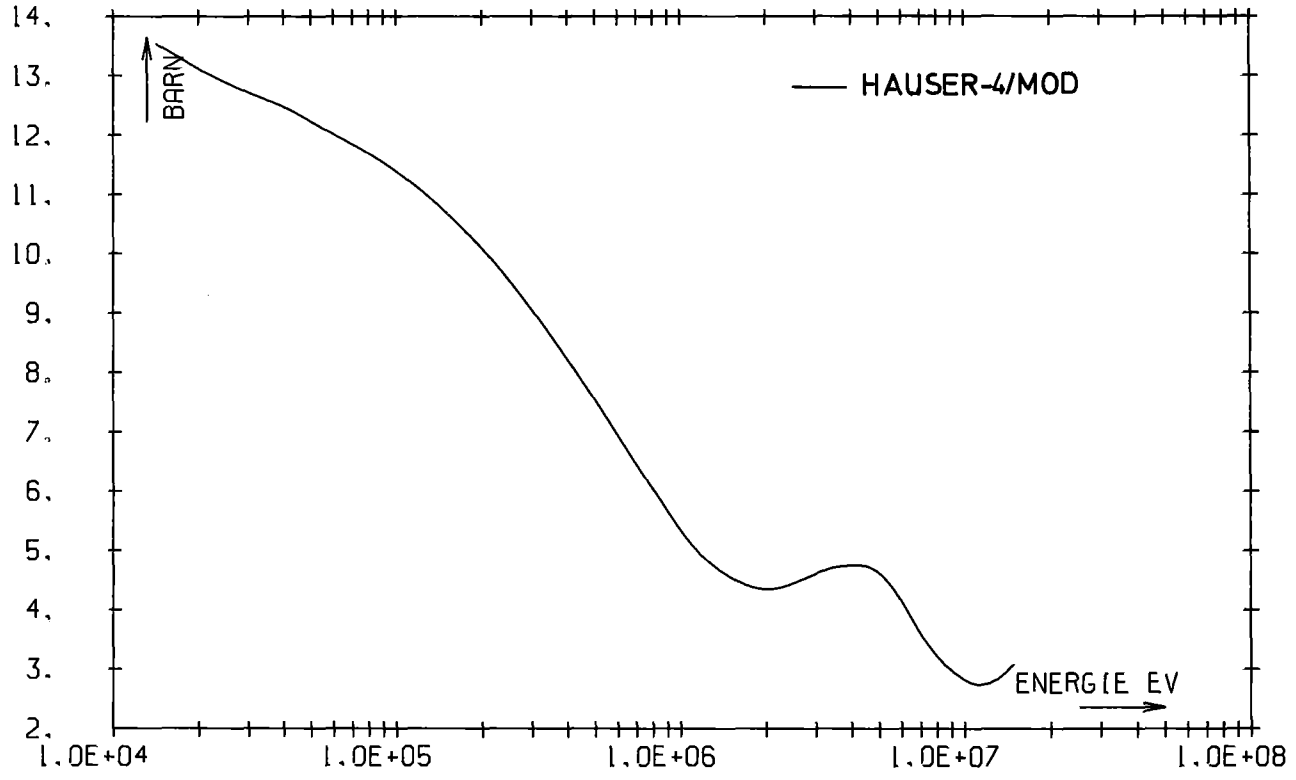

Fig. 13b Cm-244 Elastic cross-section

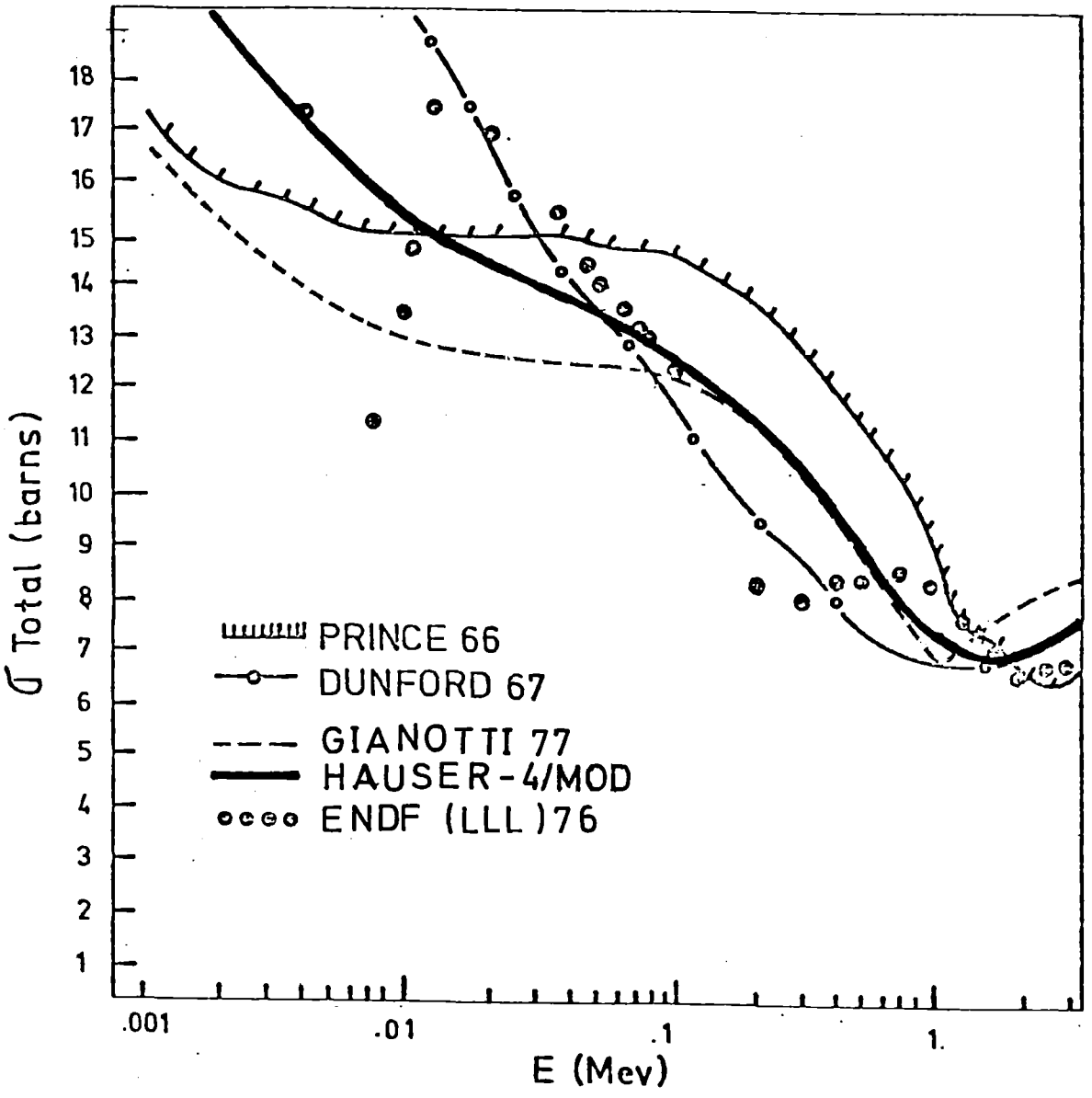

Fig. 14 Evaluated Cm-244 total cross-section compared to other evaluations /34/

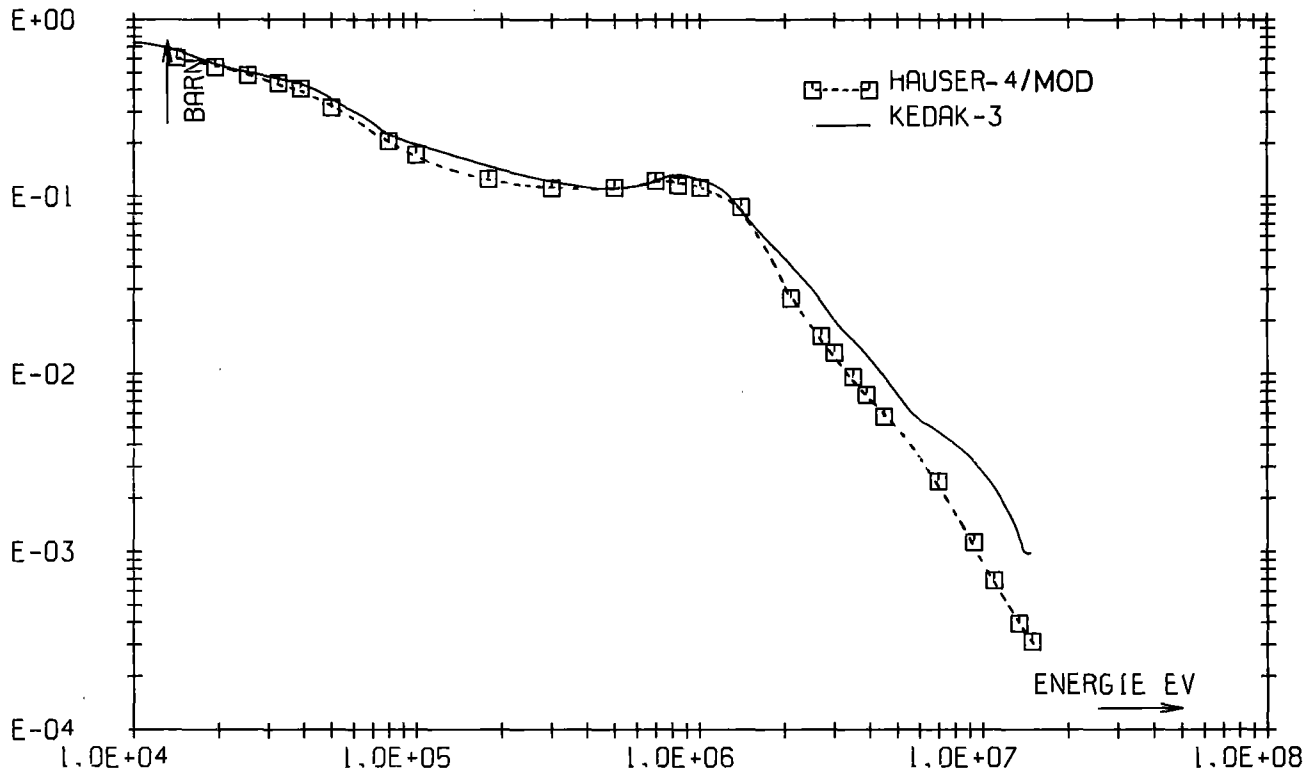

Fig. 15a U-238 capture cross-section

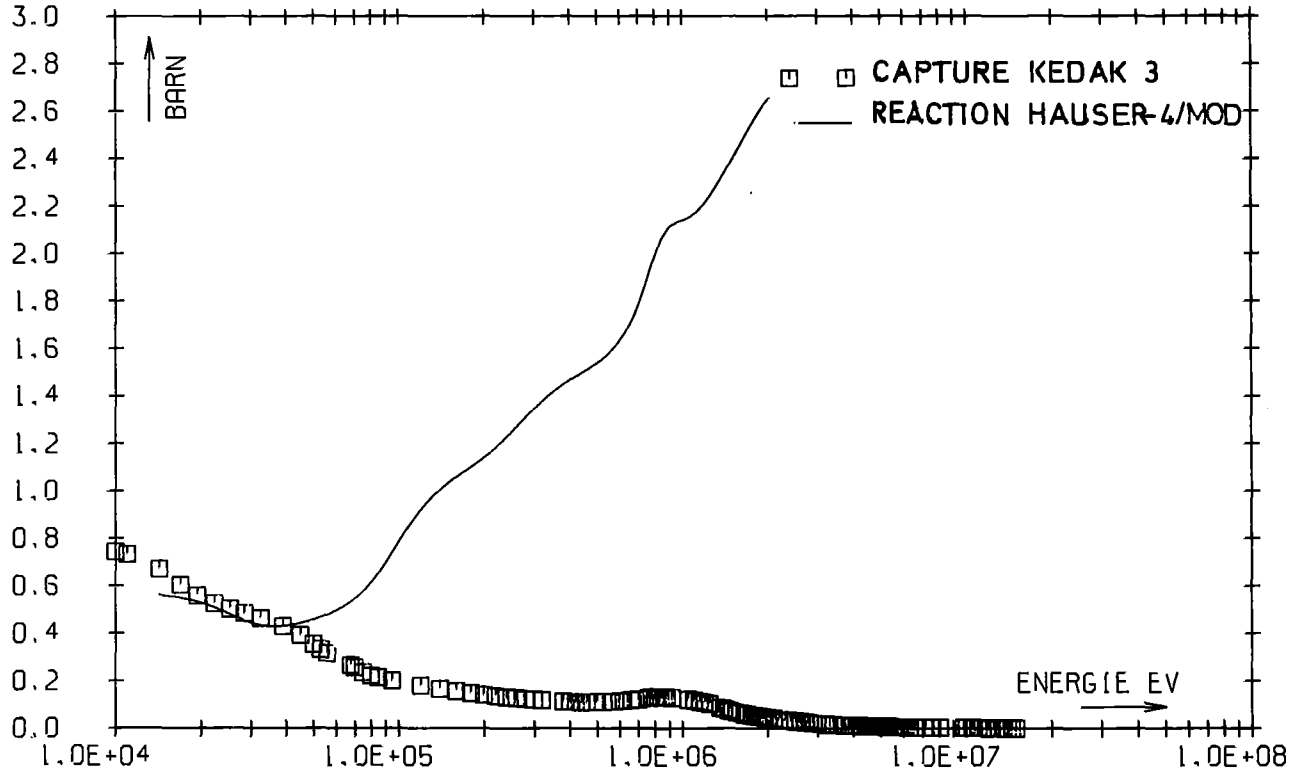

Fig. 15b U-238 Evaluated reaction cross-section and KEDAK-3 capture cross-section

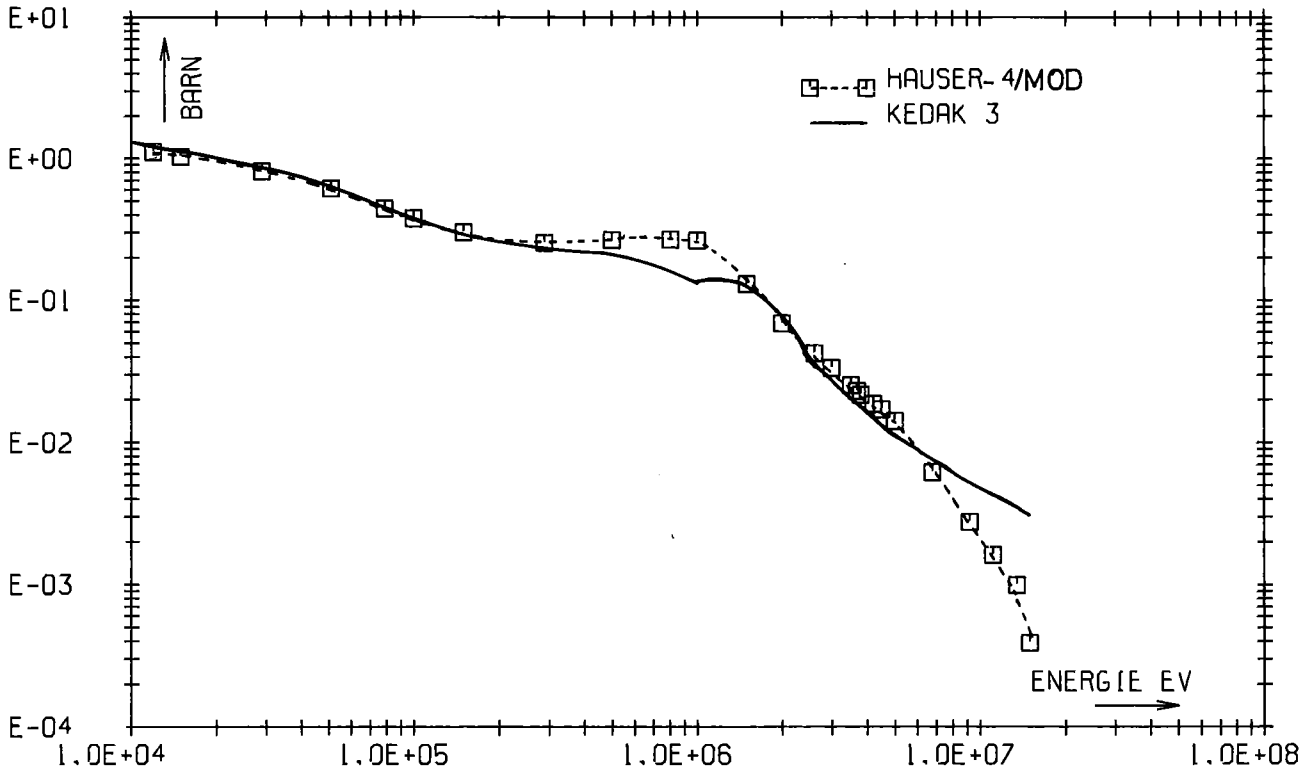

Fig. 16a Pu-240 capture cross-section

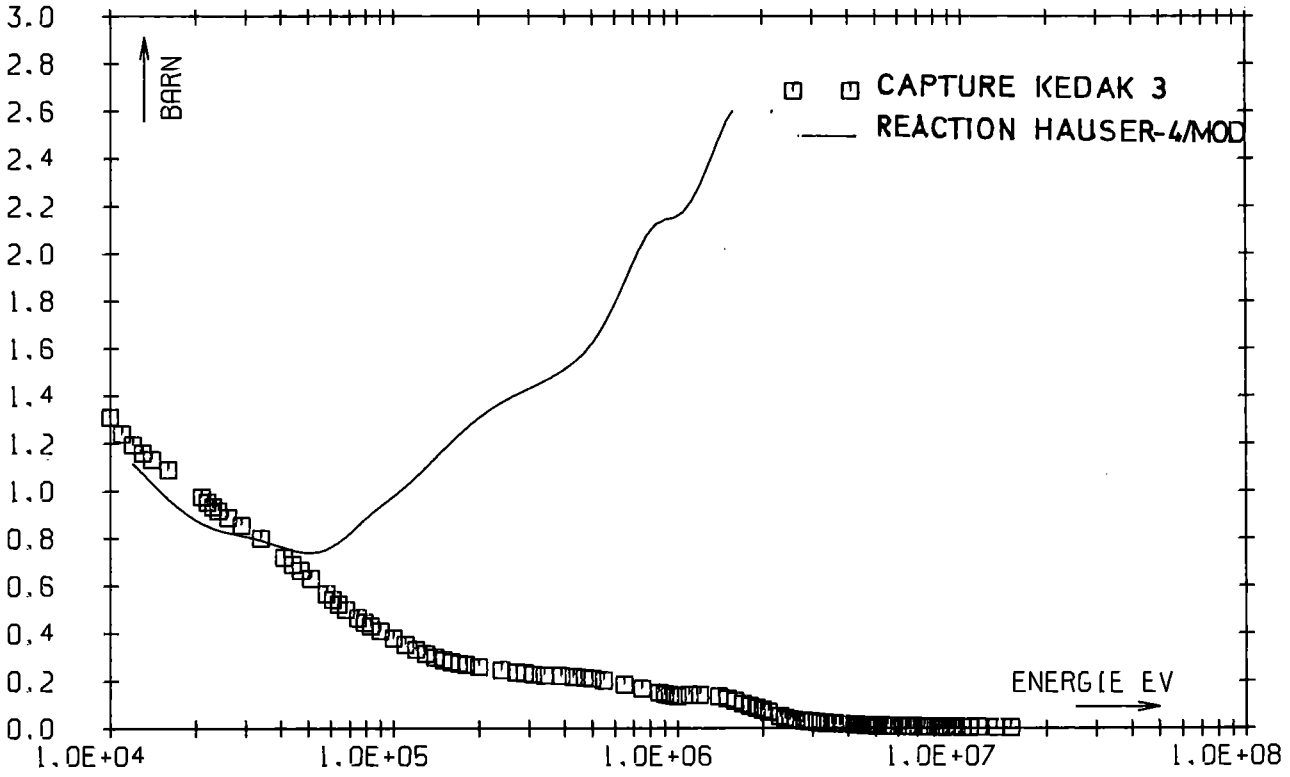

Fig. 16b Pu-240 Evaluated reaction cross-section and KEDAK-3 capture cross-section

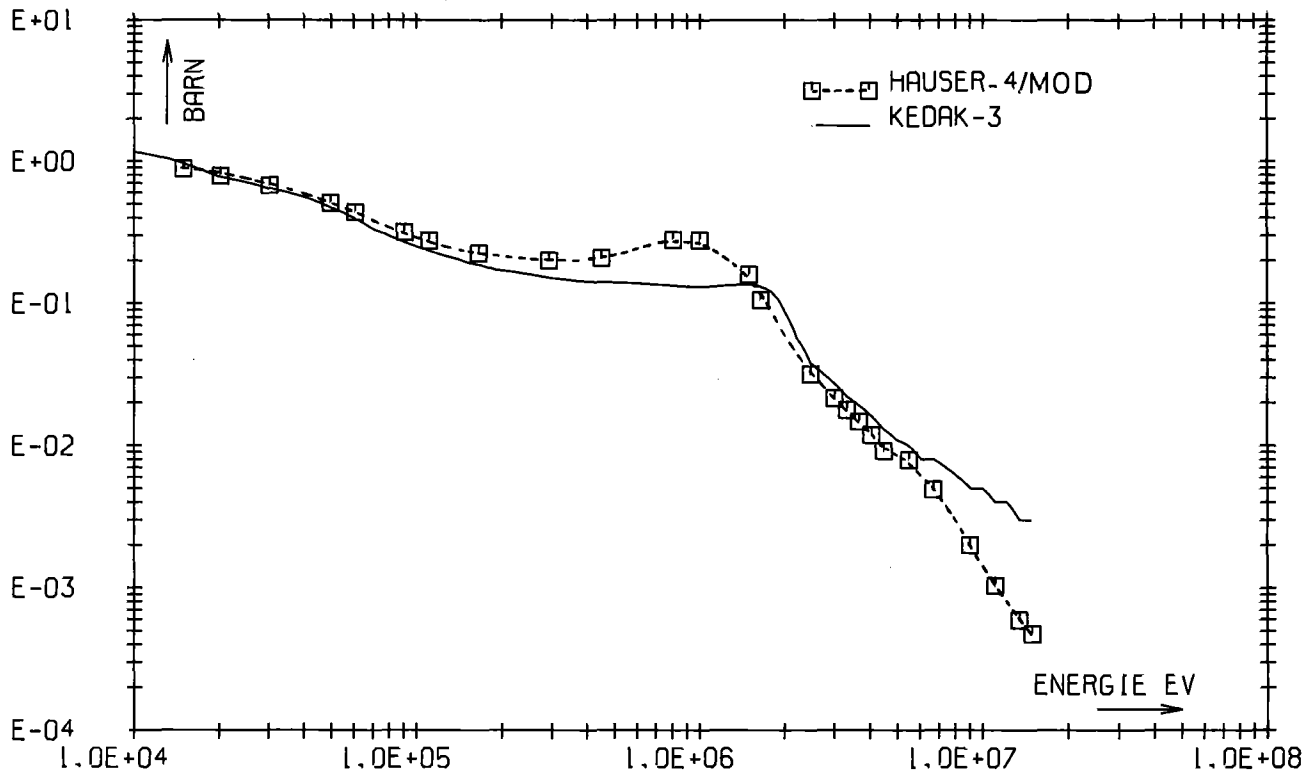

Fig. 17a Pu-242 capture cross-section

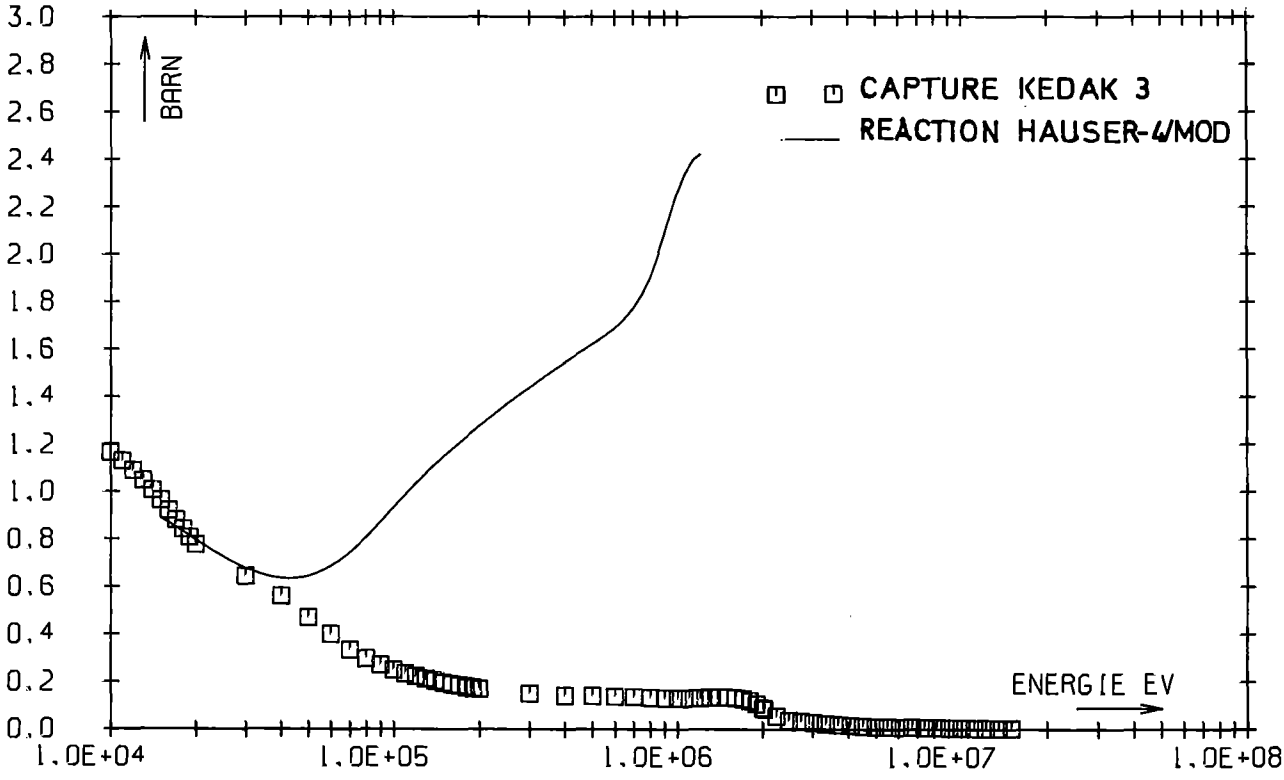

Fig. 17b Pu-242 Evaluated reaction cross-section and KEDAK-3 capture cross-section

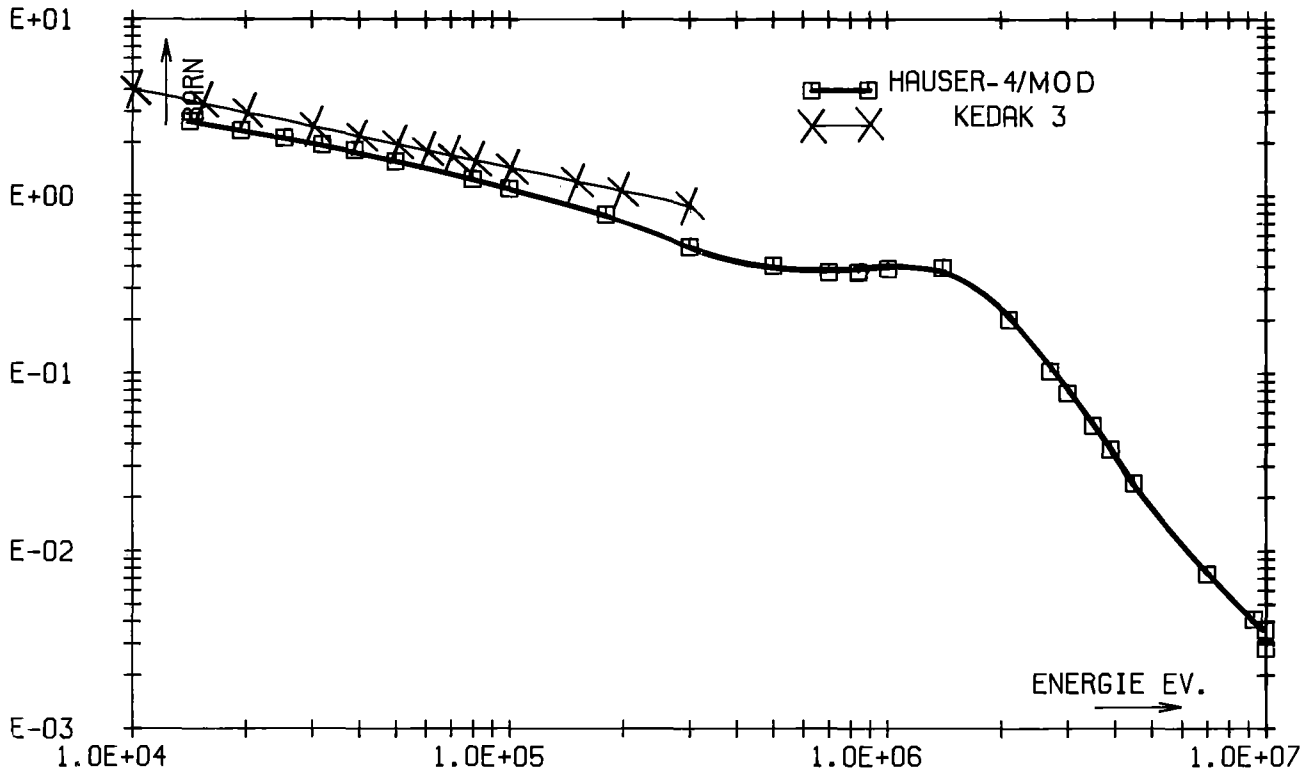

Fig. 18a **Am-241 capture cross-section**

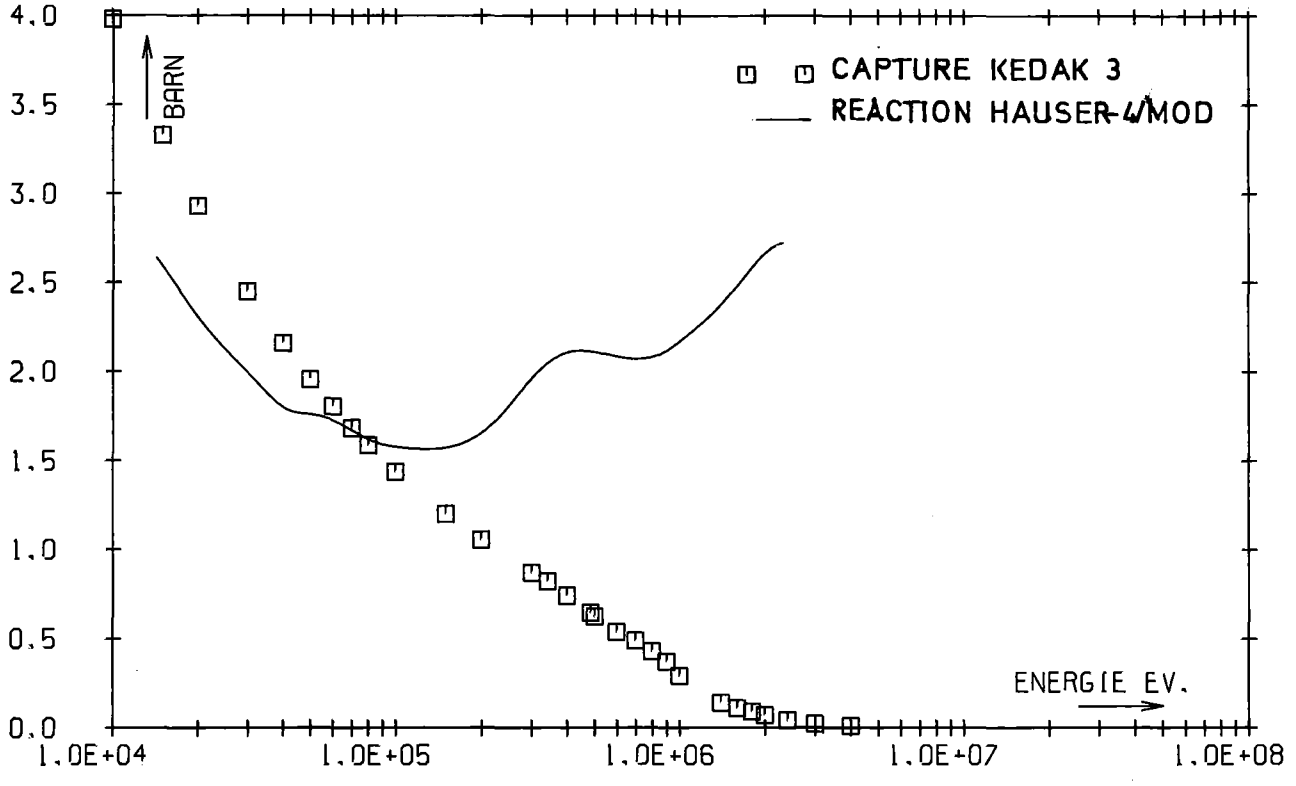

Fig. 18b **Am-241 Evaluated reaction cross-section and KEDAK-3 capture cross-section**

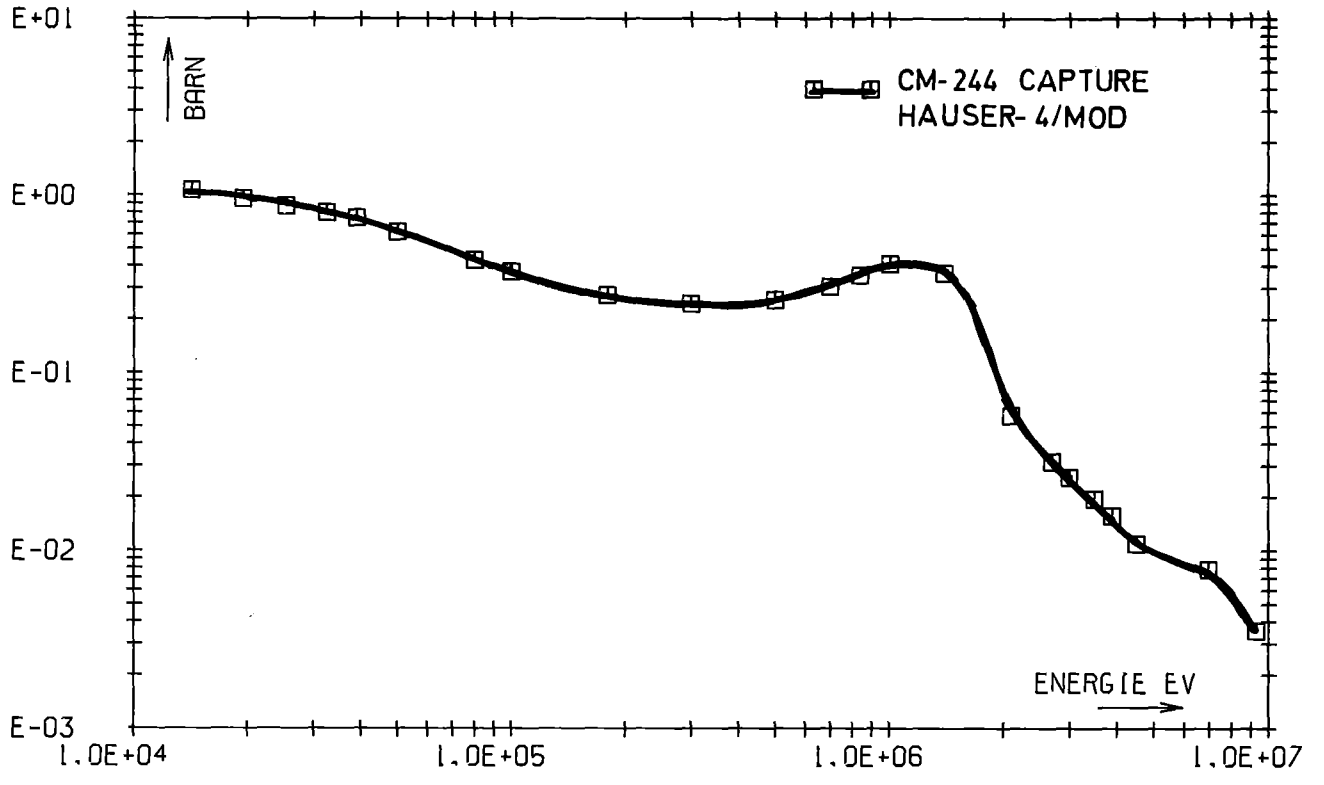

Fig. 19a Cm-244 capture cross-section

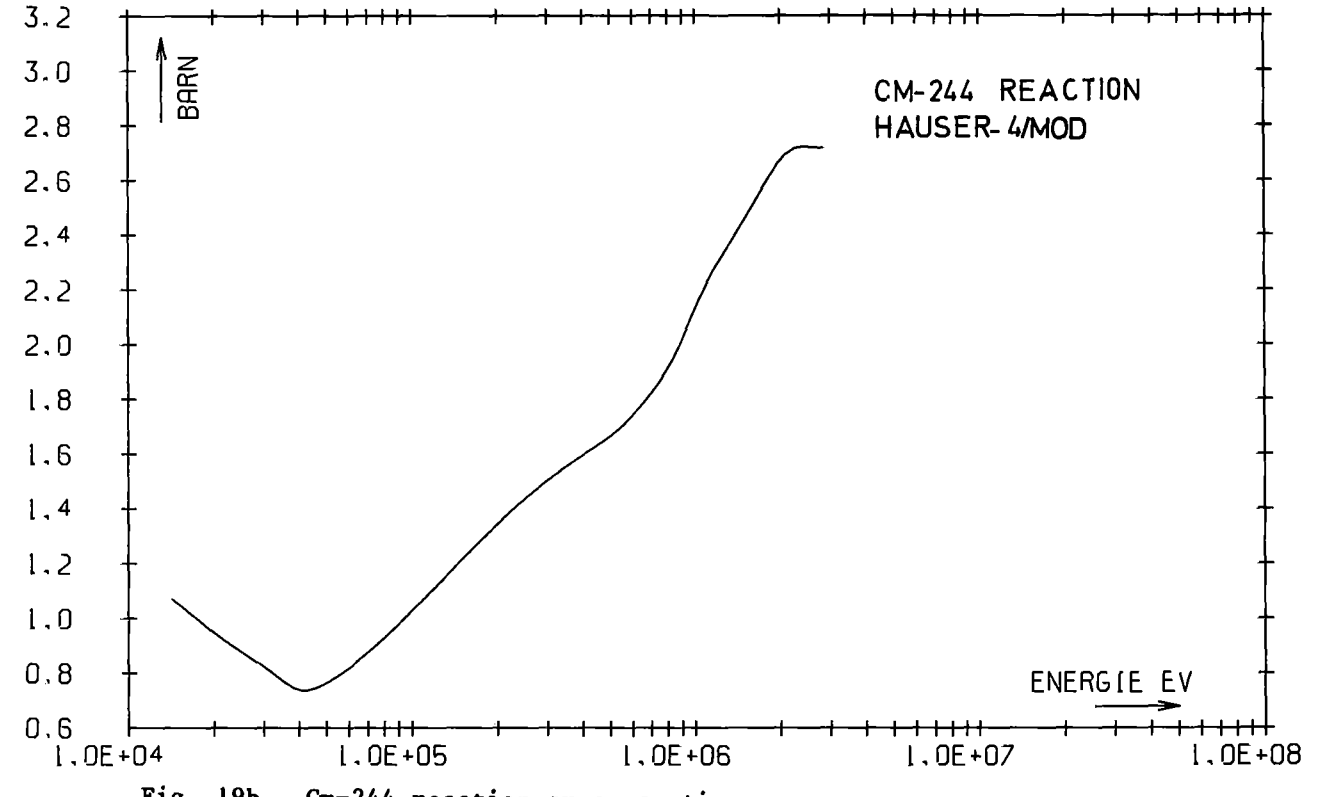

Fig. 19b Cm-244 reaction cross-section

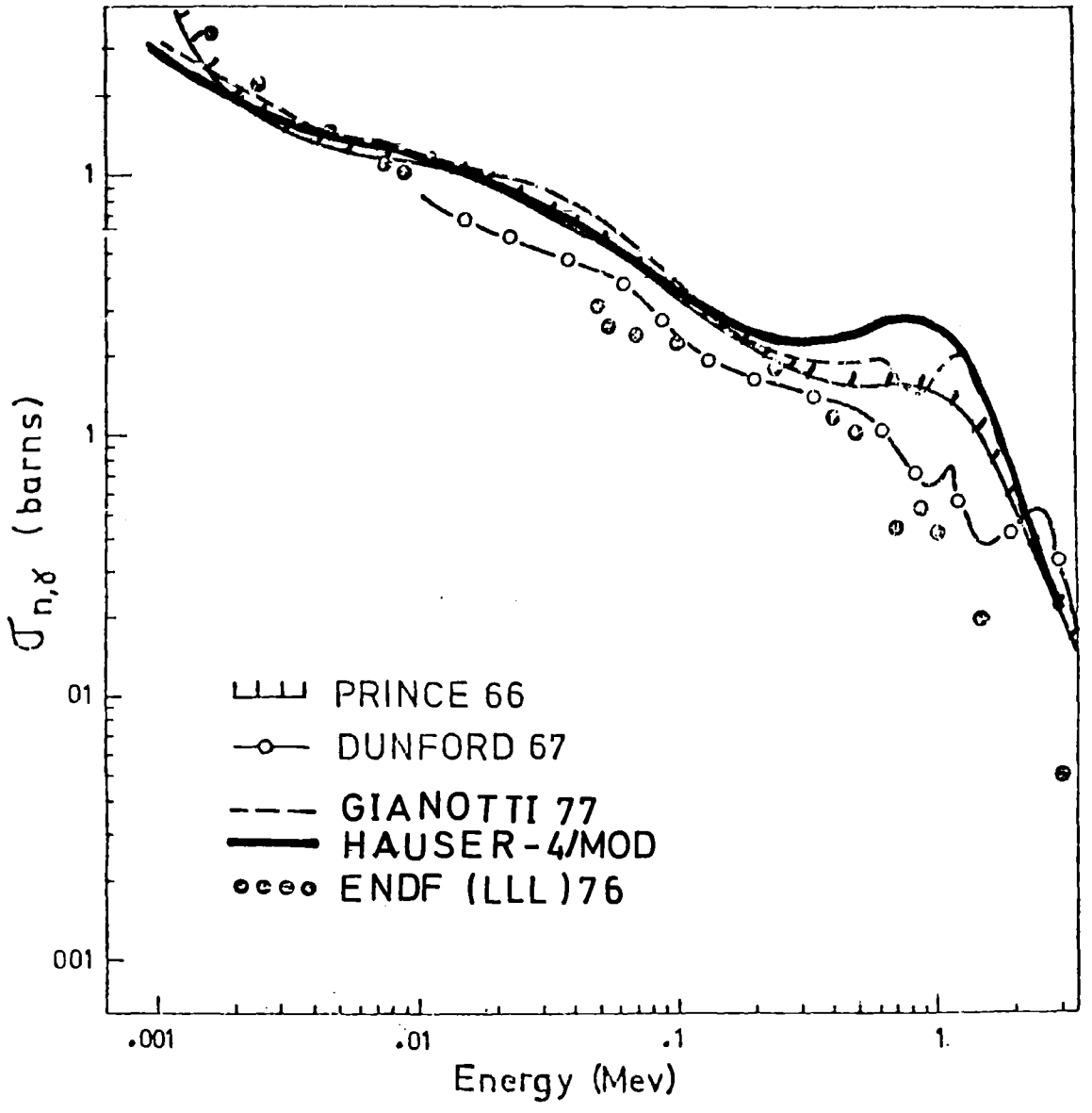

Fig. 20 Evaluated Cm-244 capture cross-section compared to other evaluations /34/

6. References

/1/ D.G. Madland, P.G. Young:
Neutron-Nucleus Optical Potential for the Actinide Region,
Los Alamos Report LA-UR-78-2510

/2/ H. Feshbach:
The Optical Model and its justification,
An. Rev. Nucl. Sci. 8(1958), 49

/3/ M.A. Preston:
Physics of the Nucleus, Addison-Wesley 1962

/4/ H.A. Bethe:
Phys. Rev. 47(1935), 747

/5/ N. Bohr: Nature 137(1936), 344
N. Bohr, F. Kalckar: Kgl. Videnskab. Selskab.,
mat.-fys. Medd. 14(1937), 10

/6/ H.H. Barshall:
Phys. Rev. 86(1952), 431

/7/ S. Fernbach, R. Serber, T.B. Taylor:
Phys. Rev. 75(1949), 1352

/8/ H. Feshbach, C.E. Porter, V.F. Weisskopf:
Model for Nuclear Reactions with Neutrons;
Phys. Rev. 96(1954), 448

/9/ A. Messiah:
Quantenmechanik Bd. 1, de Gruyter 1976

/10/ L.I. Schiff:
Quantum Mechanics, Third Edition, Mcgraw-Hill 1968

/11/ P.E. Hodgson:
The Optical Model of Elastic Scattering, Oxford, 1963

/12/ P.E. Hodgson:
Nuclear Reactions and Nuclear Structure, Oxford 1971

/13/ W. Hauser, H. Feshbach:
Phys. Rev. 87(1952), 366

/14/ F. Perey, B. Buck:
Nucl. Phys. 32(1962), 353

/15/ P.E. Hodgson, D. Wilmore:
Nucl. Phys. 55(1964), 673

/16/ J.M. Blatt, V.F. Weisskopf:
Theoretical Nuclear Physics, John Wiley & Sons 1952

/17/ F.M. Mann:
HAUSER*4, A Computer Code to Calculate Nuclear Cross Sections;
HEDL-TME 76-80, UC-796

/18/ P.H. Cowell, A.C.D. Crommelin:
Appendix to Greenwich Observatories for 1909, Edinburgh 1910

/19/ J. Fox, E.T. Goodwin:
Proc. Cambridge Phil. Soc. 45(1949), 373

/20/ M.A. Melkanoff, T. Sawada, J. Raynal:
Nuclear Model Calculations; Methods in Computational Physics 6(1966), 1

/21/ D.L. Hill, J.A. Wheeler:
Phys. Rev. 56(1953), 1102

/22/ Y.A. Ellis: Nucl. Dat. Sheets 21(1977), 549
Y.A. Ellis, R.L. Haese: Nucl. Dat. Sheets 21 (1977), 615
Y.A. Ellis: Nucl. Dat. Sheets 20(1977), 218
Y.A. Ellis: Nucl. Dat. Sheets 23(1978), 132
M.R. Schmorak: Nucl. Dat. Sheets 17(1976), 391
Y.A. Ellis: Nucl. Dat. Sheets 19(1976), 103

Y.A. Ellis: Nucl. Dat. Sheets 19(1976), 143
H.G. Börner, H.R. Koch, H. Seyfarth, T. Egidy, W. Mampe, J.A. Pinston, K. Schreckenbach, D. Heck: Study of the Level Structure of ^{239}U Using the Thermal Neutron Capture Reaction; Zeits. f. Phys. A 286 (1978), 31

/23/ J.A. Holmes, S.E. Woosley, W.A. Fowler, B.A. Zimmermann: Atomic and Nucl. Dat. Tabl. 18(1976), 306

/24/ P. Axel: Phys. Rev. 126(1962), 671

/25/ A.M. Lane, J.E. Lynn: Nucl. Phys. 11(1959), 646

/26/ H. Gilbert, A.G.W. Cameron: Can. Journ. of Phys. 43(1965), 1446

/27/ B. Goel, F. Weller: Evaluation for the German Nuclear Data Library KEDAK-3, Part 2 Fissile and Fertile Materials; KFK 2386/III

/28/ M. Caner, L. Gitter: Operating Instructions for the ABACUS/NEARREX Code; TNSD-R/419, Soreq Nucl. Research Centre, Israel

/29/ G. Schelinski, M. Strohbusch, B. Goel: Nucl. Phys. A 153(1970), 97

/30/ T.Y. Byoun, R.C. Block, T. Semler: National Topical Meeting on New Developments in Reactor Physics and Shielding 1972; Report CONF-720901 p. 1115

/31/ F.H. Fröhner: persönliche Mitteilung 1978/79

/32/ F. Käppeler: Report KFK-2223

/33/ A.B. Smith, P. Lambropoulos, J.F. Whalen: Nucl. Sci. Eng. 47(1972), 19

/34/ H.F. Gianotti:
Nucl. Sci. Eng. 65(1978), 164

/35/ T.W. Phillips, R.E. Howe:
DOE-NDC-12, p. 110

/36/ L.W. Weston, J.H. Todd:
Nucl. Sci. Eng. 63(1977), 143

/37/ K. Wisshak, F. Käppeler:
Nucl. Sci. Eng. 66(1978), 363

/38/ R.W. Hockenbury, W.R. Mayer, R.C. Block:
Nucl. Sci. Eng. 49(1972), 153

/39/ R.W. Hockenbury, A.J. Sanislo, N.N. Kaushal:
Proc. of Conference on "Nuclear Cross Sections and Technology",
Washington (1975) NBS spec. publ. 425, Vol. II, p. 584

/40/ B. Goel:
Evaluation of High Plutonium Isotopes for the German Nuclear Data File KEDAK; contributed paper to BNL Specialist Meeting on Nuclear Data for High Plutonium and Americium Isotopes for Reactor Applications, Brookhaven/Upton, Nov. 20-22 1978

/41/ M. Caner, S. Yiftah: IA-1243 (1972)
M. Caner, S. Yiftah: IA-1275 (1973)
M. Caner, S. Yiftah: IA-1276 (1973)

/42/ W. Poenitz, E. Pennington, A.B. Smith, R. Howeston:
ANL/NDM-32

/43/ E. Barnard, A.J.G. Ferguson, W.R. McMurray, I.J. van Hurden:
Nucl. Phys. 80(1966), 46

/44/ R. Batchelor, J. Towle:
Nucl. Phys. 65(1965), 236

/45/ H.H. Knitter, M. Coppola, N. Ahmed, B. Jay:
Zeits. f. Phys. 244(1971), 358

/46/ G. de Saussure, D.K. Olsen, R.B. Perez, F.C. Difilippo:
Evaluation of the ^{238}U Neutron Cross Sections for Incident Neutron Energies up to 4 keV; ORNL/TM-6152 (ENDF-257)

Acknowledgement

I am very grateful to Priv.-Doz. Dr. H. Jahn for the animation of this work and his helpful support. I also wish to thank Dr. B. Goel for his aid and many stimulating discussions and Dr. F.H. Fröhner for useful discourses and comments.

Dipl.-Ing. C.H.M. Broeders is acknowledged for his friendly aid in using the computing facility, Fr. R. Heger for adapting the code HAUSER*4 to the IBM at KfK.

Last but not least I wish to thank Fr. Bunz for her patience in typing the manuscript.